The Thesis Committee for Zhitong Luo
Certifies that this is the approved version of the following thesis:

Sliding Mode Control of the Reaction Wheel Pendulum

APPROVED BY
SUPERVISING COMMITTEE:

Supervisor:

Benito Fernandez.

Luis Sentis

Sliding Mode Control of the Reaction Wheel Pendulum

by

Zhitong Luo, B.E.

Thesis

Presented to the Faculty of the Graduate School of

The University of Texas at Austin

in Partial Fulfillment

of the Requirements

for the Degree of

Master of Science in Engineering

The University of Texas at Austin

December 2014

Dedication

To those who sacrificed themselves for a better world.

Acknowledgements

I want to give my best gratitude to my supervisor Dr. Benito Fernandez, who has help me overcome many obstacles in this research. He inspired from the start and guided me all the way to the end. Also I want to thank Dr. Luis Sentis who agreed to be my co-supervisor.

And I also want to thank members in Advanced Mechatronics Lab, Jose Capriles, Ignacio Olivares and Javier Bastidas. They have given me valuable advice all the time.

At last, I want to thank the department of mechanical engineering in The University of Texas at Austin and all faculty. All of them has helped me achieve academic excellence in the last 2 years.

Abstract

Sliding Mode Control of the Reaction Wheel Pendulum

Zhitong Luo, M.S.E

The University of Texas at Austin, 2014

Supervisor: Benito Fernandez

The Reaction Wheel Pendulum (RWP) is an interesting nonlinear system. A prototypical control problem for the RWP is to stabilize it around the upright position starting from the bottom, which is generally divided into at least 2 phases: (1) *Swing-up phase*: where the pendulum is swung up and moves toward the upright position. (2) *Stabilization phase*: here, the pendulum is controlled to be balanced around the upright position. Previous studies mainly focused on an energy method in swing-up phase and a linearization method in stabilization phase. However, several limitations exist. The energy method in swing-up mode usually takes a long time to approach the upright position. Moreover, its trajectory is not controlled which prevents further extensions. The linearization method in the stabilization phase, can only work for a very small range of angles around the equilibrium point, limiting its applicability.

In this thesis, we took the 2nd order state space model and solved it for a constant torque input generating the family of phase-plane trajectories (see Appendix A). Therefore, we are able to plan the motion of the reaction wheel pendulum in the phase

plane and a sliding mode controller may be implemented around these trajectories. The control strategy presented here is divided into three phases. (1) In the *swing up phase* a switching torque controller is designed to oscillate the pendulum until the system's energy is enough to drive the system to the upright position. Our approach is more generic than previous approaches; (2) In the *catching phase* a sliding surface is designed in the phase plane based on the zero torque trajectories, and a 2^{nd} order sliding mode controller is implemented to drive the pendulum moving along the sliding surface, which improves the robustness compared to the previous method in which the controller switches to stabilization mode when it reaches a pre-defined region. (3) In the *stabilization phase* a 2^{nd} order sliding mode integral controller is used to solve the balancing problem, which has the potential to stabilize the pendulum in a larger angular region when compared to the previous linearization methods. At last we combine the 3 phases together in a combined strategy. Both simulation results and experimental results are shown. The control unit is National Instruments CompactRIO 9014 with NI 9505 module for module driving and NI 9411 module for encoding. The Reaction Wheel Pendulum is built by Quanser Consulting Inc. and placed in UT's Advanced Mechatronics Lab.

Table of Contents

List of Tables

List of Figures

Chapter 1：Introduction

The Reaction Wheel Pendulum (RWP), which is also called Inertia Wheel Pendulum, is a classic nonlinear system in the pendulum family that also includes the furuta pendulum, inverted pendulum, cart-pole system and pendubot. In comparison to a simple pendulum, the actuator of RWP is installed at the end of the link, which brings interesting nonlinearities and coupling effects. The RWP lays the ground of many humanoid robots and rocket designs [1]. Due to the simple structure and nonlinear characteristics, it is often used to practice nonlinear control methods.

Figure 1：A furuta pendulum

Figure 2：A pendubot

The task of controlling the RWP is to bring it from bottom position to upright position and stabilize it there. Due to the limitation of the torque, The RWP is unable to maintain an arbitrary position that we usually do in a simple pendulum. Therefore, the approach of controlling the RWP usually consists of at least 2 steps. Step one is usually

called swing-up in which the system oscillates the pendulum toward upright positon. Step two is usually called stabilization in which the system stabilizes the RWP in the upright position.

Spong [2] made a significant contribution to the swing up strategy using an energy/passivity method. The energy of the wheel is defined as $S_1 = \frac{1}{2}\omega_r^2$. The required energy for the pendulum to stay in the upright position is defined as E_{ref} and the total energy of the pendulum is E. The energy storage function can be described as $S_2 = \frac{1}{2}\left(E - E_{ref}\right)^2$. Thus the energy storage function for the system can be described as $S = k_1 S_1 + k_2 S_2$. Spong selects an appropriate control input u that it is able to assure that $\dot{S} < 0$ everywhere, which means both the wheel velocity $\dot{\theta}_r \to 0$ and the total pendulum energy $E \to E_{ref}$. The latter implies that the pendulum is closing on the upright position. He also proved that the saturation due to the torque limit would not affect his approach.

Saber [3] introduced a linearization method for global stabilization that aggressively brings the pendulum from the bottom position to the upright position. However, it was proved that this method required too much torque and had no practical use.

Srinivas [4] introduced 2 methods of swing up: (1) sinusoidal swing up strategy: A damping term is injected into saber's method to reduce the torque requirement by sinusoidal movement. (2) A switching IDA-PBC (Interconnection and damping assignment with passivity based control) method was introduced to swing up and

balancing. And both methods have been compared to the energy method and proved to be more efficient as they use less numbers of swings to reach upright position.

Bapiraju [5]introduced a fuzzy logic controller for stabilization and had a successful experiment result.

Aguilar [6] created an algorithm to design a periodic motion of the RWP around the upright position. He transformed the system into the normal form for exact linearization and used Describing Function method to find an explicit expression of a two-relay controller that excites the periodic motion. He also proved that it was stable moving along the trajectory using frequency domain analysis.

In this thesis, we propose an innovative method for controlling the RWP based on a phase plane analysis. Our contributions are:

(1) Phase plane analysis: By integrating the 2^{nd} order RWP state space model, we can find the explicit math expression of the RWP trajectories in the phase plane when constant torque applied. These trajectories are then used to design a controller.

(2) Catching zone design: A catching zone is designed to assure a robust switch from the swing-up phase to the stabilization phase. Within the boundaries of the catching zone, it is guaranteed that the pendulum moves toward the upright position.

(3) Sliding mode control: We are able to use the sliding mode strategy to control the pendulum from any position to the upright position along a designed trajectory. This strategy comprises of three steps:

- Swing up

A switching torque (bang-bang) method is used to oscillate the pendulum with increasing amplitude, and the pendulum approaches the upright position. The phase plane trajectory can be explicitly solved.

The advantage of this new method is that the trajectory can be solved so that the motion of swing-up becomes controllable while the previous energy method can only guarantee that the pendulum reaches the upright position but the process is uncontrollable. Also it is unknown how PD gain parameters (k_e, k_v, k_u) affect the performance of the swing-up in the traditional energy method [1].

- Catching

Phase plane analysis is used to analyze the behavior of the pendulum. The trajectory s_0 describing how the pendulum oscillates from one upright position to another is found. When the pendulum reaches (crosses) trajectory s_0, we can use a sliding mode controller to force the pendulum to approach the upright position along trajectory s_0. The boundaries of the region within which the pendulum is able to be controlled along trajectory s_0 are explicitly solved.

The sliding mode controller in the catching zone improves the robustness between the swing-up phase and the following stabilization phase compared to the previous switching control that defines a linearized switching condition that is very hard to catch the pendulum in experiment [1].

- Stabilization

  A 2nd order sliding mode controller has been designed to achieve balancing robustness without the extra work involved with observer or adaptive methods. The discontinuous term in the sliding mode control is proved to be able to compensate the disturbances and motor dynamics.

  The sliding mode controller requires less tune-up effort while it is hard to find a good combination of several gain parameters (k_{dp}, k_{pp}, k_{dr}) in previous linearization PD controller. The sliding mode stabilization controller also has the potential to balance the pendulum around the upright position in a larger angle range, which may be desired in other robotic applications.

At last, we compare the simulation and experimental result using the RWP in the Advanced Mechatronics Lab in The University of Texas. Discussions of the advantage of our method over previous methods are also included.

Chapter 2：Modelling

2.1 Conventional Reaction Wheel Pendulum Model

The Reaction Wheel Pendulum is a nonlinear underactuated system with 2 degrees of freedom. Compared to a conventional pendulum, the difference is the actuator placed at the end of the link. The schematic diagram is shown in Figure 3. Both pendulum coordination and wheel coordination are defined clockwise from vertical axis. The parameters are listed in Table 1.The friction on the pendulum shaft is included as F. The differential equations of the motion was addressed in [1] as following:

$$\ddot{\theta} = \frac{d_{22}}{\det D}\bar{m}g\sin(\theta) - \frac{d_{12}}{\det D}\tau - F \tag{1}$$

where

$$d_{11} = m_1 l_1^2 + m_2 l_2^2 + I_1 + I_2,$$

$$d_{12} = d_{21} = d_{22} = I_2,$$

$$detD = d_{11}d_{22} - d_{12}d_{21}$$

$$\bar{m} = m_1 l_1 + m_2 l_2$$

Table 1：Parameters of RWP

Descriptions	Symbols	Units
Mass of the pendulum	m_1	kg
Mass of the wheel	m_2	kg
Distance from the pivot to the center of mass of the pendulum	l_1	m
Distance from the pivot to the center of mass of the wheel	l_2	m
Moment of inertia of the pendulum	I_1	kgm^2
Moment of inertia of the wheel	I_2	kgm^2

2.2 WHEEL DYNAMICS

When using absolute coordinates, the wheel dynamics can be simply treated as a double integrator. The effects of coulomb friction and ball bearing friction are neglected [1].

$$\ddot{\theta}_r = \frac{1}{d_{12}}\tau \tag{2}$$

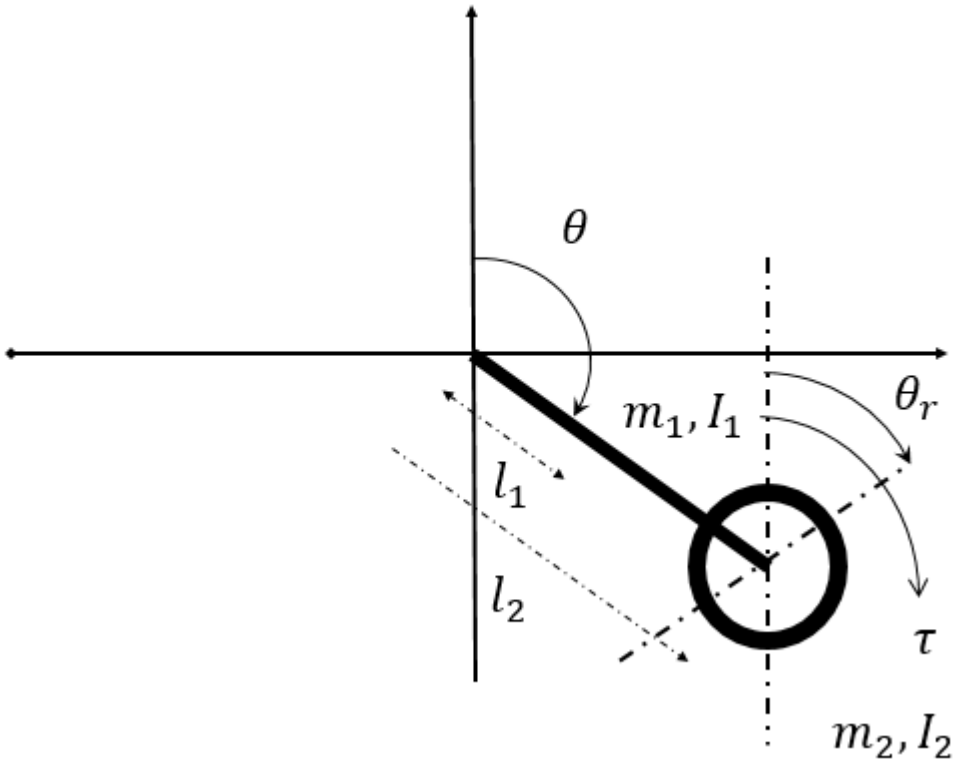

Figure 3：RWP schematic diagram. The angular position of wheel is defined as θ_r. The angular position of pendulum is defined as θ. Their angular velocities are defined as $\dot{\theta}_r$ and $\dot{\theta}$, respectively. Both θ_r and θ are clockwise and measured from a fixed vertical base.

2.3 MOTOR DYNAMICS

Motor dynamics [1] can be written as

$$L\frac{dI}{dt} + RI = V - k_e\dot{\theta}_r \tag{3}$$

Where L and R are the armature inductance and resistance, respectively. k_e is the motor back EMF constant and V is the applied voltage.

A 2nd order sliding mode controller is designed in the following chapters with torque control. And we want the actual torque output of the motor follows the desired torque we calculated from the controller. We select the torque τ as our variable of interest. Substitute $\tau = kI$, and (3) becomes

$$\dot{\tau} = \frac{k_e}{L}V - \frac{R}{L}\tau - \frac{{k_e}^2}{L}\dot{\theta}_r \tag{4}$$

Combining Equation (3) and (4), the motor dynamics is a linear system so that it can be described by transfer function and block diagram, which is shown in Figure 4. Assume the desired torque we calculated from sliding mode controller is τ_r and the actual control input of motor is the voltage V that is achieved using PWM.

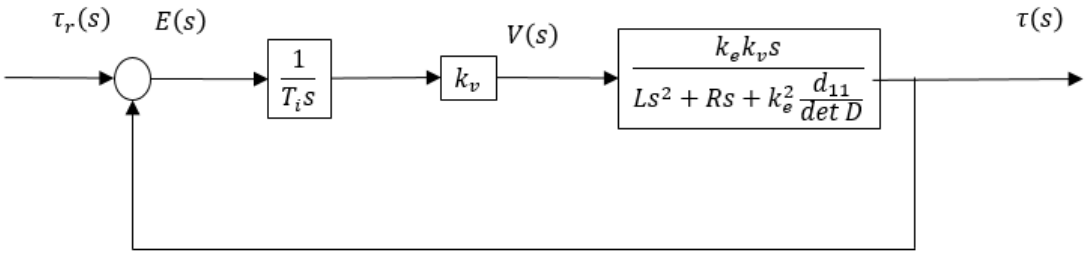

Figure 4: Block diagram of motor dynamics. It is an open loop second order system. τ_r is the desired torque. τ is the actual torque output of the motor. k_v is the ratio of voltage V over desired torque τ_r.

Combining motor dynamics and the pendulum model, the Reaction Wheel Pendulum system can be described as 5th order nonlinear differential equations. $x_1 = \theta_1,\ x_2 = \dot{\theta}_1, x_3 = \theta_r\ ,\ \ x_4 = \dot{\theta}_r,\ x_5 = \tau$

$$\dot{x}_1 = x_2$$

$$\dot{x}_2 = a\sin(x_1) - \mathrm{b}x_5 - F$$

$$\dot{x}_3 = x_4$$

$$\dot{x}_4 = cx_5$$

$$\dot{x}_5 = \frac{k_e}{L}V - \frac{{k_e}^2}{L}x_4 - \frac{R}{L}x_5 \qquad (5)$$

where

$$a = \frac{d_{22}}{\det D}\bar{m}g$$

$$\mathrm{b} = \frac{d_{12}}{\det D}$$

$$c = \frac{1}{d_{12}}$$

Equation (5) can be rewritten to matrix form as

$$\dot{x} = f(x) + g(x)u$$

$$f(x) = \begin{bmatrix} x_2 \\ a\sin x_1 - bx_5 - F \\ x_4 \\ cx_5 \\ -\frac{k_e^2}{L}x_4 - \frac{R}{L}x_5 \end{bmatrix}$$

$$g(x) = \begin{bmatrix} 0 \\ 0 \\ 0 \\ 0 \\ \frac{k_e}{L} \end{bmatrix}$$

$$u = V \tag{6}$$

When ignored motor dynamics, Equation (5) can be reduced to a second order system

$$\dot{x}_1 = x_2$$

$$\dot{x}_2 = a\sin(x_1) - \mathrm{b}\tau - F \tag{7}$$

Chapter 3：Swing-up

The first step is to initiate the pendulum oscillation with increasing amplitude. Since the motor torque is very limited, it cannot bring the pendulum to the upright position from bottom position in one swing. That is to say, an oscillatory motion is required. Previous study by Spong [2] focused on an energy method and passivity control.

One major challenge in swing up control is that the RWP is a nonlinear system in large amplitude oscillation when the small angle approximation is no longer applicable. The 2nd order differential Equations (7) do not have a generalized explicit solution for the angular position of pendulum with finite terms, which makes it impossible to tracking any explicit swing up trajectory.

In this section, a switching control law is used to swing up the pendulum. The simplest control is a switching law of the form:

$$\tau = -\tau_0 \operatorname{sgn}(x_2) \tag{8}$$

This control law has two modes with constant torque.

With a constant torque the system can be integrated into a 1st order differential equation, which provides opportunity of phase plane analysis. The detailed calculation is listed in the Appendix A. The swing-up motion can be described as

$$\phi(x_1, x_2) = \frac{1}{2}x_2^2 + a\cos(x_1) - \mathrm{b}\tau_0 \operatorname{sgn}(x_2)x_1 + c_1 = 0 \tag{9}$$

where c_1 is the arbitrary constant in integration based on initial conditions. If $x_1(t=0) = \theta_0,\ x_2(t=0) = \omega_0$,

$$c_1 = -\frac{1}{2}\omega_0^2 - a\cos\theta_0 + b\tau_0\theta_0\,\mathrm{sgn}(\omega_0)$$

The system is able to accumulate energy and move close to the upright position by switching the direction of torque when the angular velocity reduced to zero, as described in Equation (8). An example of phase plane is shown in Figure 5

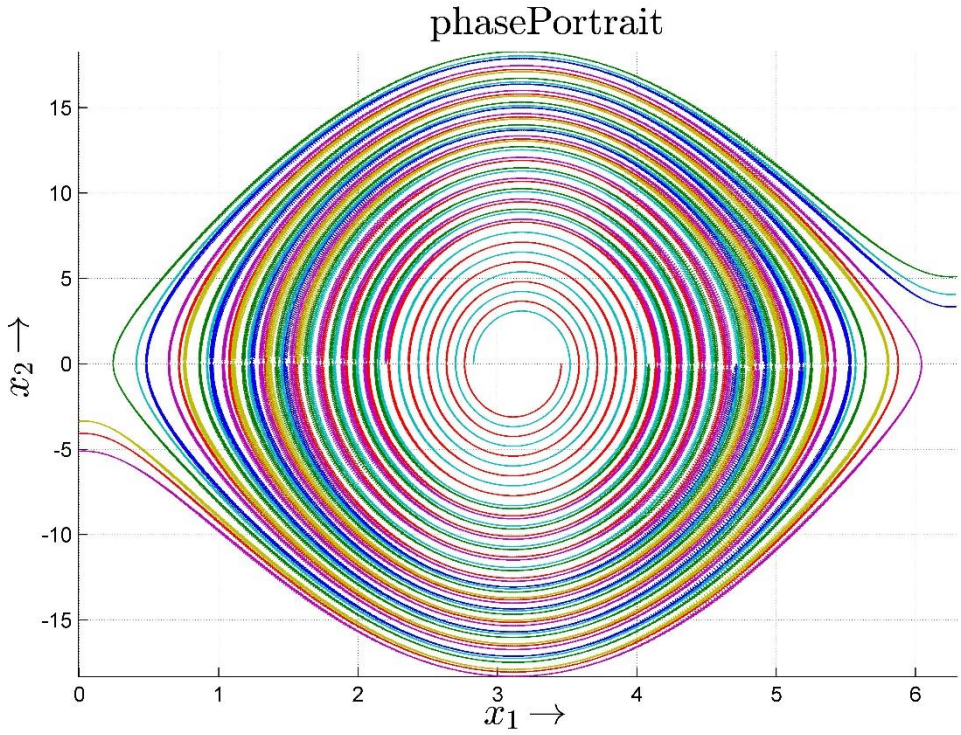

Figure 5：Swing up strategy diagram in phase plane. Six different initial conditions are evenly divided to from $\left(\frac{\pi}{2}, 0\right)$ to $\left(\frac{3}{2}\pi, 0\right)$. Three of them reach the upright position $x_1 = 0$ and the others reach $x_1 = 2\pi$

Chapter 4: Catching

In the previous section, the pendulum is able to conduct an oscillatory motion and move closer to the upright position from bottom position. When it reaches certain angular position and velocity, it is able to move to upright position in current swing. In this section, we discuss the region in which the control strategy can catch the pendulum from the swing up mode and drive it toward the upright position along a unactuated free swing trajectory. The phase plane analysis is used.

4.1 Maximum Stabilization Angle

Given the usual limitation of the motor torque, the RWP can only be stabilized in the upright position locally. Now our target is to find the angle where the maximum torque is equal to the gravity term of the pendulum. That is to say that the torque is able to overcome the gravity effect inside this angle range, otherwise the pendulum yields to the gravity and falls down.

The difference between upright and bottom position is that the gravity pulls the pendulum away from the unstable equilibrium points $(\pm 2n\pi, 0)$ while the gravity pulls it toward the stable equilibrium points $(\pm(2n+1)\pi, 0)$ at the bottom position. Assume the maximum static offset of pendulum angle is θ_{max}, i.e. angular velocity and angular acceleration are both zero, and maximum torque applied is $\tau_{\max}$. From Equation (7)

$$\ddot{\theta} = a\sin(\theta_{max}) - b\tau_{\max} \tag{10}$$

When $\ddot{\theta} = 0$, the maximum angle offset can be calculated as

$$\theta_{max} = \arcsin\left(\frac{\tau_{max}}{\bar{m}g}\right) \tag{11}$$

4.2 CATCHING ZONE

In order to consider both the position and velocity we describe the catching zone in phase plane. One important trajectory is the one that pendulum oscillates from one upright position to another upright position with friction neglected and no torque applied, which is plotted in the Figure 6. The trajectory can be described by

$$s_0 = -\frac{1}{2}\dot{\theta}^2 + a(1 - \cos\theta)=0 \tag{12}$$

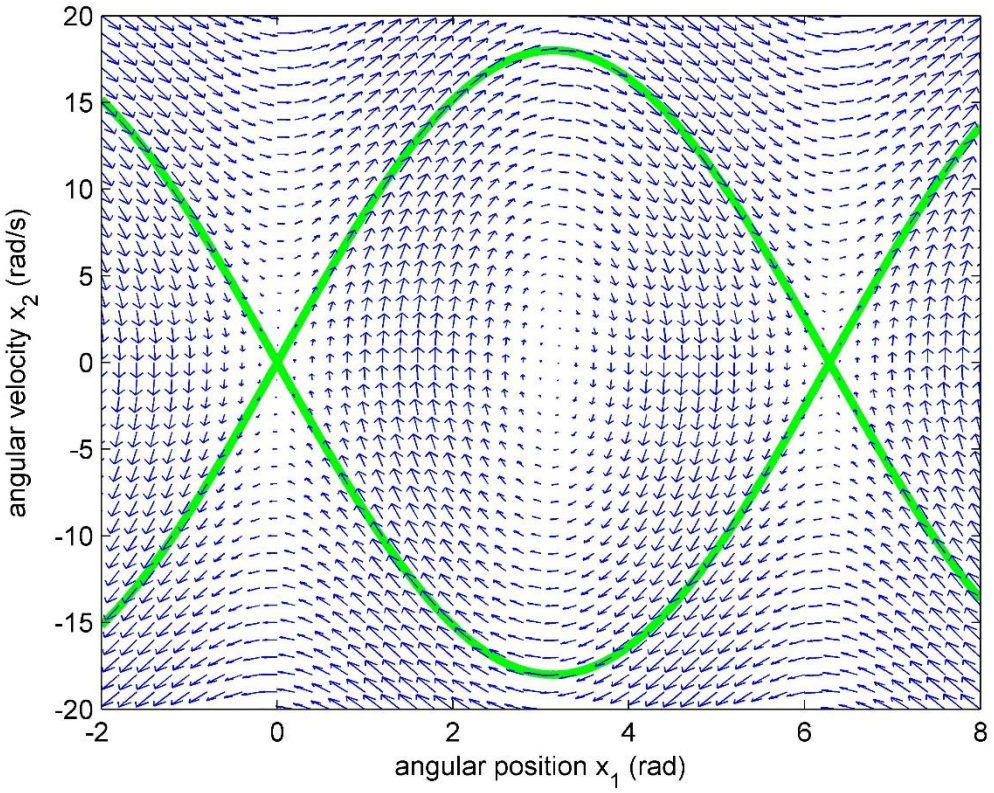

Figure 6：The green line describes the trajectory that the pendulum swings from one upright position to another if the friction is neglected. The phase portrait shows the pendulum behavior with no torque applied and friction neglected from arbitrary initial conditions. The working range in our thesis is between (0, 0) and $(2\pi, 0)$

The trajectory above the $x_2 = 0$ axis describes the pendulum moving toward $(2\pi, 0)$ with positive velocity and the one below describes the pendulum moving toward (0, 0) with negative velocity. The working range of our pendulum is between 0 and 2π. From

the phase portrait we noticed that (0, 0) and $(2\pi, 0)$ are unstable equilibrium points and $(\pi, 0)$ is stable equilibrium points.

To find the boundary of catching, we assume the pendulum is moving toward (0, 0) and the trajectory of the pendulum moving toward $(2\pi, 0)$ can be ignored. In this way, $\omega_0 < 0$. It has 2 circumstances: (1) The velocity $|\omega_0|$ is less than that along trajectory s_0 at the same angular position, which is shown as it is above the trajectory s_0 in the Figure 7. The boundary of this case is that the trajectory ends at $(\theta_{max}, 0)$ when τ_{max} applied, which is shown as the blue line labeled as s_1 which can be described as

$$s_1 = -\frac{1}{2}\omega_0^2 + a(\cos\theta_{max} - \cos\theta) + b\tau_{max}(\theta_{max} - \theta) \tag{13}$$

(2) The velocity $|\omega_0|$ is greater than that along the trajectory s_0 at the same angular position, which is shown as it is below the free swing trajectory in the Figure 7. The boundary of this case is that the trajectory ends at $(-\theta_{max}, 0)$ when $-\tau_{max}$ applied, which is shown as the red line labeled as s_2 which can be described as

$$s_2 = -\frac{1}{2}\omega_0^2 + a(\cos\theta_{max} - \cos\theta) - b\tau_{max}(-\theta_{max} - \theta) \tag{14}$$

Now we can obtain a region between s_1 and s_2. And the conditions that the pendulum are able to be stabilized around the original point (0, 0) can be described as

$$s_{x\to 0} = \{s_1 \le 0 \cap s_2 \ge 0 \cap x_2 \le 0\} \tag{15}$$

The region representing Equation (15) is shown in the Figure 7.

Similarly, we can find the region regarding to stabilizing at (0, 2π). At this time the maximum angle offsets where the maximum torque is equal to gravity term are

$2\pi - \theta_{max}$ and $2\pi + \theta_{max}$. The boundary that ends at $(2\pi + \theta_{max}, 0)$ with positive maximum torque τ_{max} can be described as

$$s_3 = -\frac{1}{2}\omega_0^2 + a(\cos\theta_{max} - \cos\theta) + b\tau_{max}(2\pi + \theta_{max} - \theta) \tag{16}$$

The boundary that ends at $(2\pi - \theta_{max}, 0)$ with negative maximum torque $-\tau_{max}$ can be described as

$$s_4 = -\frac{1}{2}\omega_0^2 + a(\cos\theta_{max} - \cos\theta) - b\tau_{max}(2\pi - \theta_{max} - \theta) \tag{17}$$

And the region that the pendulum is able to be stabilized around $(2\pi, 0)$ can be described as

$$s_{x\to 2\pi} = \{s_3 \geq 0 \cap s_4 \leq 0 \cap x_2 \geq 0\} \tag{18}$$

The region representing Equation (18) is shown in the Figure 8.

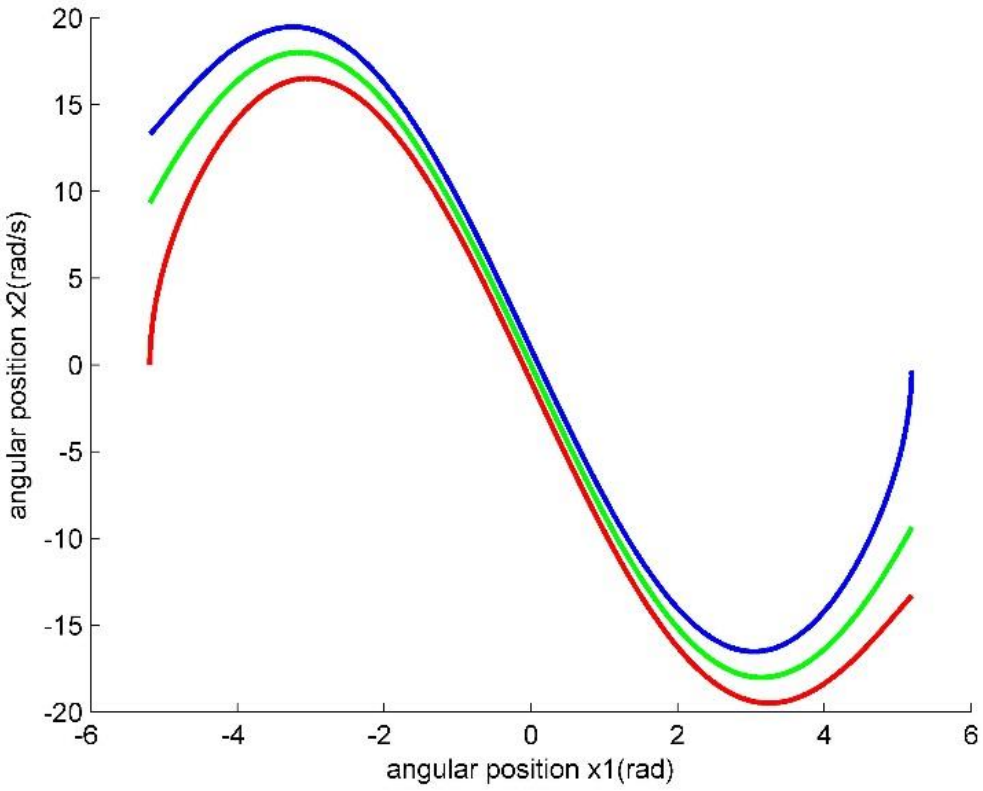

Figure 7：The figure displays the catching region of stabilization around original point (0, 0). The blue line represents the boundary s_1 in Equation (13). The red line represents the boundary s_2 in Equation (14). The green line represents trajectory s_0 in Equation (12). The region between blue line and red line is the one designed in Equation (15)

If we include the friction the boundary trajectories will not have an explicit solution but we are able to find the numerical solutions by integrating the Equation (7) backward in time. The results are shown in Figure 8 and Figure 9.

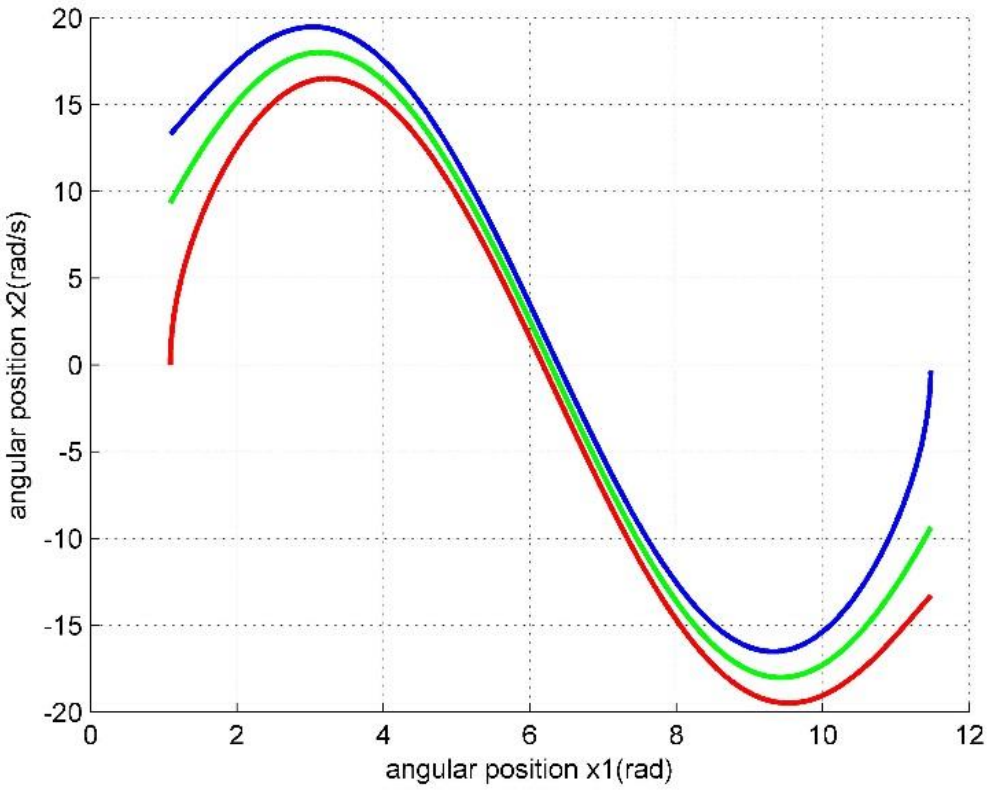

Figure 8：The figure displays the catching region of stabilizing at original point $(2\pi, 0)$ without friction. The blue line represents the boundary s_3 in Equation (16). The red line represents the boundary s_4 in Equation (17). The green line represents the trajectory s_0 in Equation (12). The region between blue line and red line is the one designed in Equation (18)

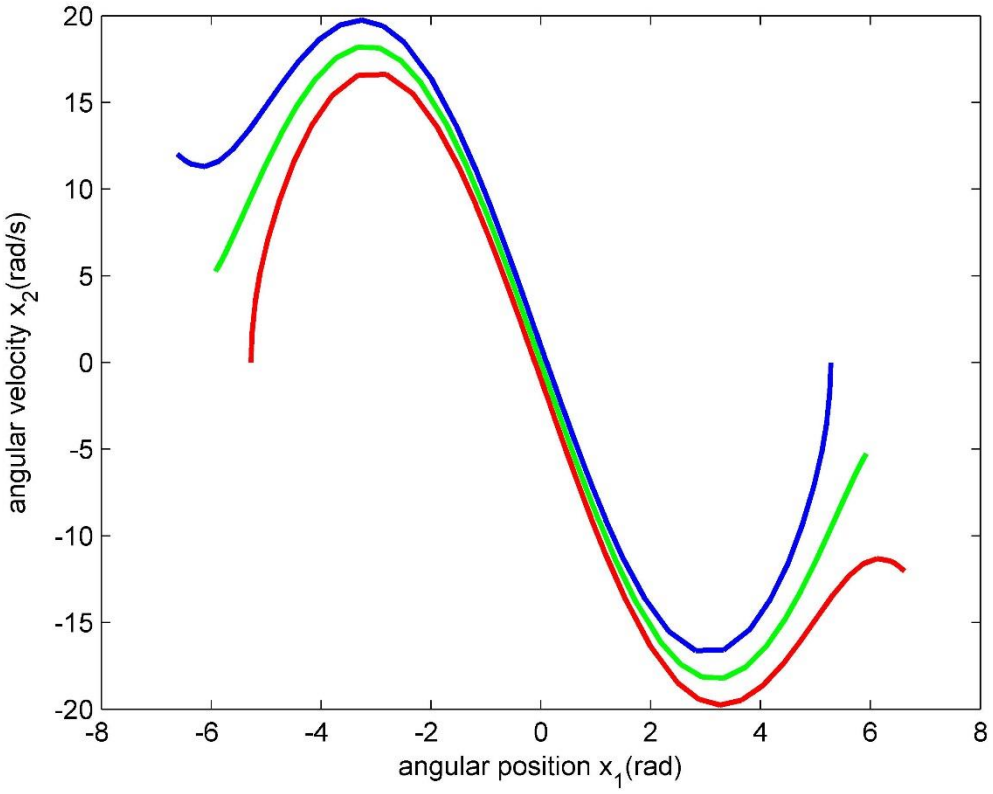

Figure 9：The figure displays the catching region of stabilizing at original point $(0,0)$ with friction. The blue line represents the boundary s_1 including friction. The red line represents the boundary s_2 including friction. The green line represents the trajectory s_0 in Equation (12). The region between blue line and red line is the one designed in Equation (18)

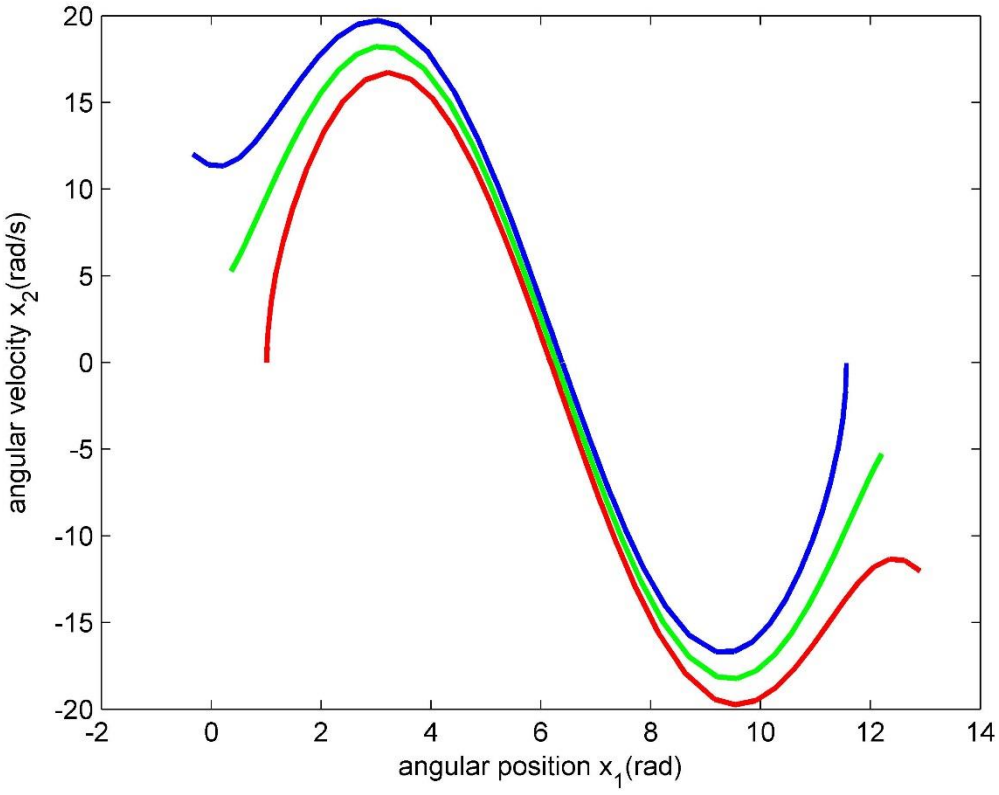

Figure 10：The figure displays the catching region of stabilizing at original point $(2\pi, 0)$ with friction. The blue line represents the boundary s_3 in Equation (16). The red line represents the trajectory s_4 in Equation (17). The green line represents the trajectory s_0 in Equation (12). The region between blue line and red line is the one designed in Equation (18)

4.3 SLIDING MODE CONTROL

After the pendulum gets into the catching zone, it is able to move toward the upright position and stabilize there. It takes least torque to bring the pendulum to

upright position along trajectory s_0. When the pendulum reaches the trajectory s_0, we switch to a sliding mode control. From Equation (12),

$$\dot{s}_0 = 0 \Rightarrow \hat{\tau} = 0 \tag{19}$$

The sliding mode controller is defined as

$$\tau = \hat{\tau} - \eta \operatorname{sgn}(s_0) \tag{20}$$

Chapter 5: Stabilization

When the pendulum reaches the upright position along the free swing trajectory, it becomes a stabilization problem. To maintain the pendulum at the upright position, a reference signal of pendulum angle x_1 is defined as $r(t)$. And

$$r^{(i)}(t) = 0 \text{ or } 2\pi$$

where derivatives $i = 0,1,2, \ldots$

The sliding surface is

$$s = \left(\frac{d}{dt} + \lambda\right)^2 \left(\int_0^t \tilde{x}\, dr\right) \tag{21}$$

Where $\tilde{x} = x_1 - r$

Add a discontinuous term to our equivalent control.

$$\dot{s} = -\eta sgn(s)$$

$$\ddot{\tilde{x}}_1 + 2\lambda\dot{\tilde{x}}_1 + \lambda^2\tilde{x}_1 = -\eta sgn(s)$$

$$\ddot{x}_1 - \ddot{r} + 2\lambda(\dot{x}_1 - \dot{r}) + \lambda^2(x_1 - r) - \eta\,\mathrm{sgn}(s)$$

Substituting $\ddot{x}_1$ by Equation (7),

$$\tau = \frac{1}{b}[a \sin x_1 - F - \ddot{r} + 2\lambda(x_2 - \dot{r}) + \lambda^2(x_1 - r)] - \eta\,\mathrm{sgn}(s) \tag{22}$$

Remark: Detailed sliding mode controller design can be found in [7]

Chapter 6：Simulation and Experiments

6.1 EXPERIMENT ENVIRONMENT

6.1.1 Hardware

The experiment hardware is performed at the Advanced Mechatronics Lab in The Department of Mechanical Engineering of The University of Texas at Austin. The RWP hardware is shown in Figure 11, which is built by Quanser Consulting Inc. The kit includes a motor with maximum torque $\tau_{\max} = 0.05$ [Nm]. Other motor parameters are shown in the Table 2. It also includes two 1000 CPR encoders, one installed on motor shaft and the other installed on the pendulum shaft.

Table 2：Parameters of Pittman motor 8222

Parameter	Value	Unit
Terminal Resistance	12.1	Ohms
Inductance	6.27	mH
Peak Torque	0.051	Nm
Torque Constant	0.027	Nm/A
Coulomb Friction Torque	0.0025	Nm

Figure 11：The RWP used in Advanced Mechatronics lab in The University of Texas at Austin

To achieve maximum resolution, we choose to use X4 encoding. The process is shown in Figure 12. In this method both rising and falling edge of Channel A and Channel B are considered to be trigger. And the direction is decided by which channel

leads the other.

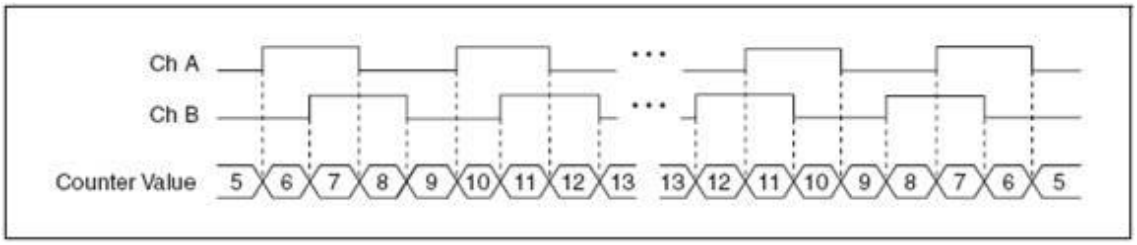

Figure 12: X4 Encoding

The resolution of the encoder using X4 encoding is

$$res = \frac{2\pi}{4CPR} = 0.00157 \ \texttt{[rad]}$$

6.1.2 Software

We choose to a CompactRIO from National Instruments as our control unit along with NI 9505 module for motor driving and NI 9411 module for encoder sampling. The basic architecture is shown in Figure 13. There are 2 ways to program the CompactRIO module.

- Scan interface mode

This mode provides maximum flexibility for developers. It skips the FPGA module and directly access to I/O, which saves a lot of time from compiling the FPGA diagram. However, the scan rate cannot go higher than 1 [kHz].

- FPGA interface mode

This mode provides maximum performance and reliability. It has no limitation on loop rate under the hardware clock (40[MHz]). However, it requires long time to compile the FPGA diagram. And the disk space in FPGA is limited.

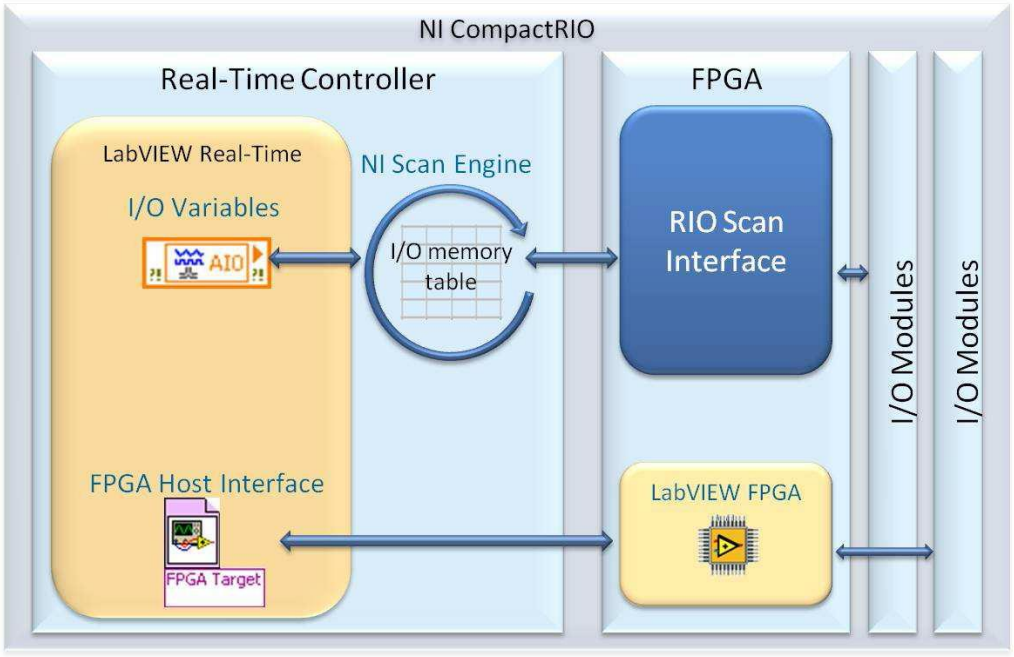

Figure 13：Basic architecture of CompactRIO

In this project, we selected the FPGA interface mode for programming because the discontinuous term in the sliding mode controller needs to be fast enough to compensate the errors. Due to the limitation of the space in FPGA, we only program the switching term of sliding mode inside the FPGA which is the most time-critical and rest of code is placed in the RT controller.

6.2 PARAMETERS ESTIMATION

In order to eliminate measurement errors in motor inertia and pendulum link length, three experiments are conducted to verify the RWP parameters a and b as well as the friction on the pendulum shaft F. From previous studies, a linear approximation of the friction is accurate enough [1]. The friction is modeled as linear $F = \mu x_2$ where μ is the friction coefficient.

1) Estimation of a

A small angle unactuated swing is experimented as no torque applied around the bottom position $x_1 = \pi$. The results are shown in the Figure 14. With friction modeled as linear, Equation (7) is rewritten as

$$\dot{x}_1 = x_2$$

$$\dot{x}_2 = a\sin(x_1) - \mu x_2 \tag{23}$$

Within a small amplitude around $x_1 = \pi$, $\sin(x_1) \approx \pi - x_1$

$$\dot{x}_1 = x_2$$

$$\dot{x}_2 = a(\pi - x_1) - \mu x_2 \tag{24}$$

The response of this 2nd order differential equation can be solved as

$$x_1 = c_1 e^{-\frac{\mu}{2}t}\cos(kt) + c_2 e^{-\frac{\mu}{2}t}\sin(kt) + \pi \tag{25}$$

$$x_2 = e^{-\frac{\mu}{2}t}\left[\left(kc_2 - \frac{\mu}{2}c_1\right)\cos(kt) - \left(kc_1 + \frac{\mu}{2}c_2\right)\sin(kt)\right] \tag{26}$$

Where $k = \frac{\sqrt{4a-\mu^2}}{2} \approx \sqrt{a}$ as $a \gg \mu$. c_1 and c_2 are arbitrary constants based on initial conditions.

In this experiment, initial conditions are defined as $x_1(0) = x_0,\ x_2(0) = 0$. And

$$c_1 = x_0 - \pi$$

$$c_2 = \frac{\mu}{k}(x_0 - \pi)$$

And Equation (24) can be rewritten to be

$$x_1 = (x_0 - \pi)e^{-\frac{\mu}{2}t}\cos\left(\sqrt{a}t\right) + \frac{\mu}{2\sqrt{a}}(x_0 - \pi)e^{-\frac{\mu}{2}t}\sin\left(\sqrt{a}t\right) + \pi \tag{27}$$

$$x_2 = -e^{-\frac{\mu}{2}t}\frac{\mu^2 + a}{4\sqrt{a}}(x_0 - \pi)\sin\left(\sqrt{a}t\right) \tag{28}$$

The parameter a can be estimated by measuring the period of the oscillation using the data shown in the Figure 14.

$$a = \omega^2 = \left(\frac{2\pi}{T}\right)^2 = 81.0637\ \ [1/\mathrm{s}^2]$$

2) Estimation of friction coefficient

To find the friction coefficient we can measure the decrease of pendulum amplitude by examining the points where the pendulum reaches the local maximum on one side. It is shown as an envelope in the Figure 14.

Mathematically, it can be explained from Equation (28)

$$\sqrt{a}t = 0{,}2\pi, 4\pi$$

$$t_i = \frac{2\pi}{\sqrt{a}}i \tag{29}$$

Where $i = 0{,}1{,}2$ ...

Substituting Equation (25) by Equation (27), all points in the envelope can be described as

$$x_i = (x_0 - \pi)e^{-\frac{\mu}{2}t_i} + \pi$$

To find the friction coefficient μ

$$x_{i+1} = (x_0 - \pi)e^{-\frac{\mu}{2}t_{i+1}} + \pi$$

$$\frac{x_{i+1} - \pi}{x_i - \pi} = \frac{e^{-\frac{\mu}{2}t_{i+1}}}{e^{-\frac{\mu}{2}t_i}} = e^{-\frac{\mu}{2}(t_{i+1} - t_i)} = e^{-\frac{\mu}{2}\Delta t}$$

$$\mu = \frac{2}{\Delta t}\ln\left(\frac{x_i - \pi}{x_{i+1} - \pi}\right)$$

Take ten points and find the average

$$\bar{\mu} = \frac{2}{9\Delta t}\ln\left(\frac{x_1 - \pi}{x_{10} - \pi}\right) = 0.1153 \ \ [1/s]$$

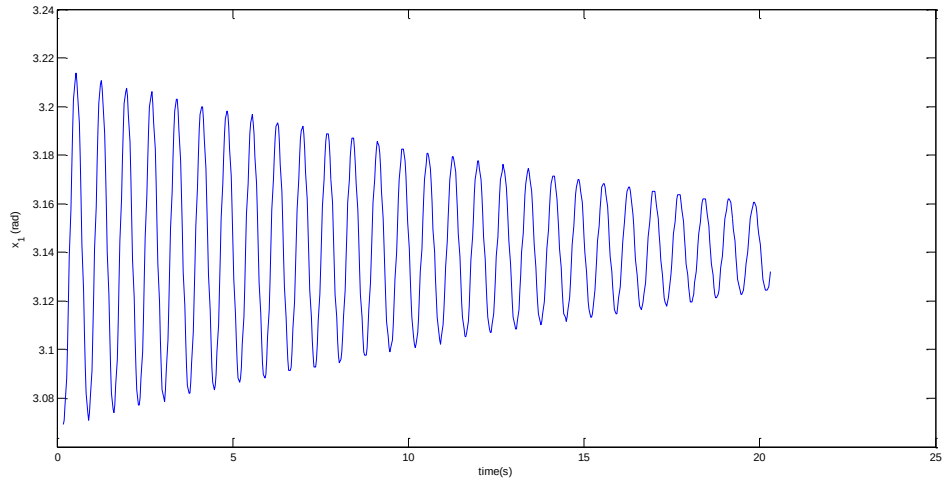

Figure 14：Pendulum angular position response with no torque applied starting from $x_1 = 3.064, \quad x_2 = 0$. We can calculate the parameter a by measuring period T and friction coefficient μ by finding differences between local maximum in one side.

3) Estimation of b

A small toque is applied when the pendulum is resting in the bottom position. Equation (7) can be reduced to

$$\dot{x}_1 = x_2$$

$$\dot{x}_2 = a(\pi - x_1) - \mathrm{b}\tau_0 - \mu x_2$$

whose trajectory can be derived as

$$x_1(t) = c_1 e^{-\frac{\mu}{2}t}\cos(kt) + c_2 e^{-\frac{\mu}{2}t}\sin(kt) + \pi - \frac{b}{a}\tau_0 \tag{30}$$

$$x_2(t) = e^{-\frac{\mu}{2}t}\left[\left(kc_2 - \frac{\mu}{2}c_1\right)\cos(kt) - \left(kc_1 + \frac{\mu}{2}c_2\right)\sin(kt)\right] \tag{31}$$

where $k = \frac{\sqrt{4a-\mu^2}}{2} \approx \sqrt{a}$. c_1, c_2 are arbitrary constants defined by the initial condition. In this experiment, initial conditions $x_1(0) = \pi,\ x_2(0) = 0$

$$c_1 = \frac{b}{a}\tau_0$$

$$c_2 = \frac{\mu b}{2a\sqrt{a}}\tau_0$$

And substitute $c_1,\ c_2$ into Equation (28) and (29). They become

$$x_1(t) = \frac{b}{a}\tau_0 e^{-\frac{\mu}{2}t}\cos\left(\sqrt{a}t\right) + \frac{\mu b}{2a\sqrt{a}}\tau_0 e^{-\frac{\mu}{2}t}\sin\left(\sqrt{a}t\right) + \pi - \frac{b}{a}\tau_0 \tag{32}$$

$$x_2(t) = -\left(\frac{b\sqrt{a}}{a} + \frac{bu^2}{4a\sqrt{a}}\right)e^{-\frac{\mu}{2}t}\sin\left(\sqrt{a}t\right) \tag{33}$$

Compare the experiment data with simulation data in Figure 15 by examining the first local maximum, i.e. the angular position when the velocity reduces to zero at the first

time. We only select the first local minimum because the following local maximum values are compromised by the motor dynamics. Assume the time elapsed is t_1

$$x_2(t_1) = -\left(\frac{b\sqrt{a}}{a} + \frac{bu^2}{4a\sqrt{a}}\right) e^{-\frac{\mu}{2}t_1} \tau_0 \sin\sqrt{a}t_1 = 0$$

$$t_1 = \frac{\pi}{\sqrt{a}}$$

And the angular position at t_1 can be calculated as

$$x_1(t_1) = \frac{b}{a}\tau_0 e^{-\frac{\mu}{2}t_1} \cos\left(\sqrt{a}t_1\right) + \frac{\mu b}{2a\sqrt{a}}\tau_0 e^{-\frac{\mu}{2}t_1} \sin\left(\sqrt{a}t_1\right) + \pi - \frac{b}{a}\tau_0$$

$$x_1(t_1) = -\frac{b}{a}\tau_0 e^{-\frac{\mu}{2}\frac{\pi}{\sqrt{a}}} + \pi - \frac{b}{a}\tau_0 \tag{34}$$

We selected 5 different τ_0= {0.02, 0.025, 0.03, 0.035, 0.04} and their first local maximum $x_1(t_1)$= {3.22013, 3.24212, 3.26254, 3.28611, 3.30967}. The average of b is

$$\bar{b} = 166.3013\ [\mathrm{rad}/\ (\mathrm{Nm}\cdot\mathrm{s}^2)]$$

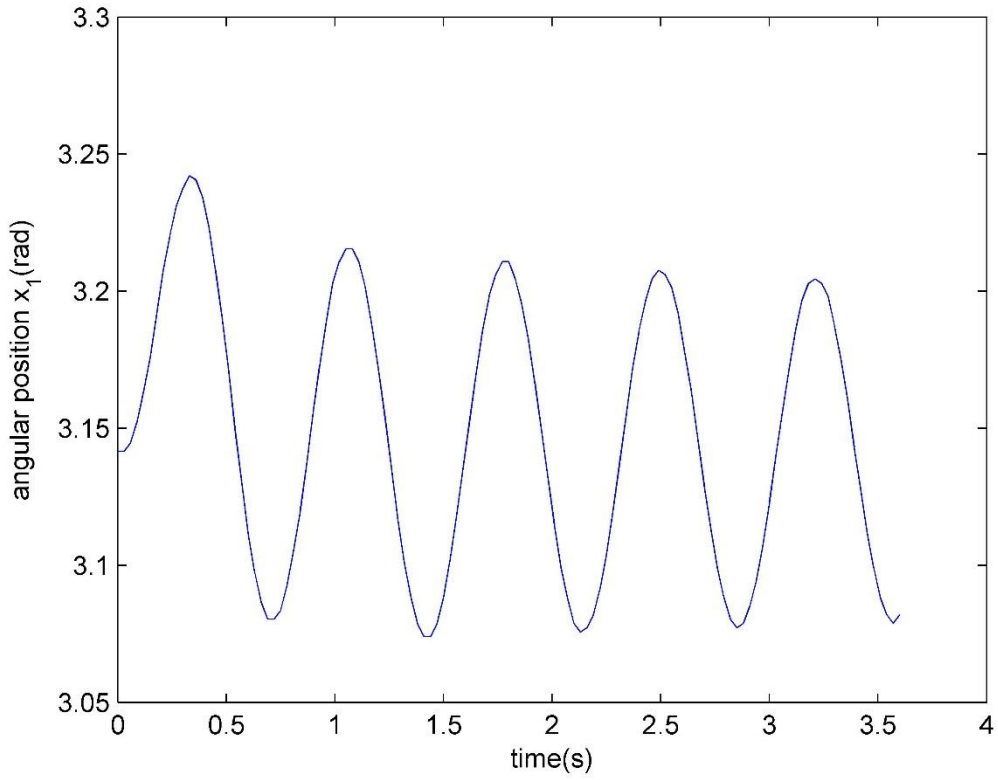

Figure 15：An example of pendulum response from the bottom position. The first local maximum in positive side is 3.24212. The torque applied is 0.025 [Nm]

6.3 CONTROLLABILITY

The controllability of the system can be found from Equation (6). The controllability matrix is constructed as

$$C = [\mathbf{g}, \mathrm{ad}_{\mathbf{f}}\mathbf{g}, \mathrm{ad}_{\mathbf{f}}^{2}\mathbf{g}, \mathrm{ad}_{\mathbf{f}}^{3}\mathbf{g}, \mathrm{ad}_{\mathbf{f}}^{4}\mathbf{g}]$$

where $\mathrm{ad}_{\mathbf{f}}^{\mathrm{i}}\mathbf{g}$ is the lie bracket of **f** and **g**. i is the recursive index. The detailed explanation is included in Appendix B.

Using the parameters we estimated from last chapter and Table 2,

$$rank(C) = 5$$

which means the system is controllable everywhere.

6.4 RESULTS

6.4.1 Swing up

Swing up is achieved by a switching controller described in Equation (8). Simulation results and experiment results are shown in Figure 12.

$$\tau_0 = 0.4\tau_{max} \approx 0.02 \ \ [\mathrm{Nm}]$$

The pendulum will reach the upright position in approximately 6 seconds with angular velocity about 5 rad/s without implementing catching algorithm.

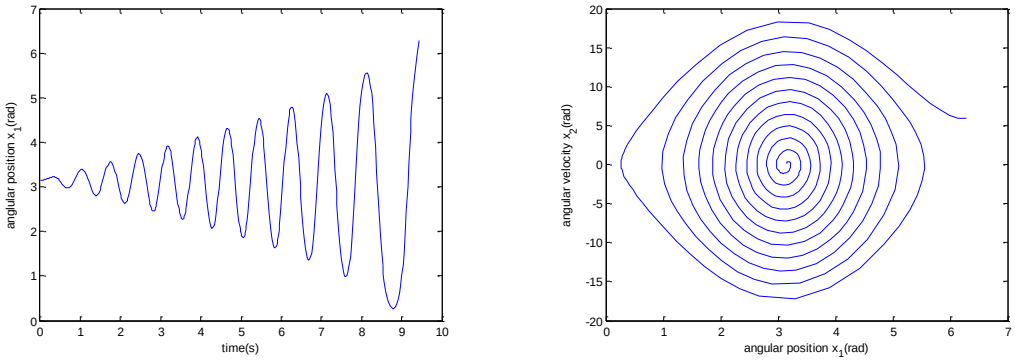

(a) (b)

Figure 16: Simulation results, excited by torque 0.02 [Nm] from $(\pi, 0)$. (a) Simulation result of pendulum angular position. (b) Simulation result of pendulum response in phase plane

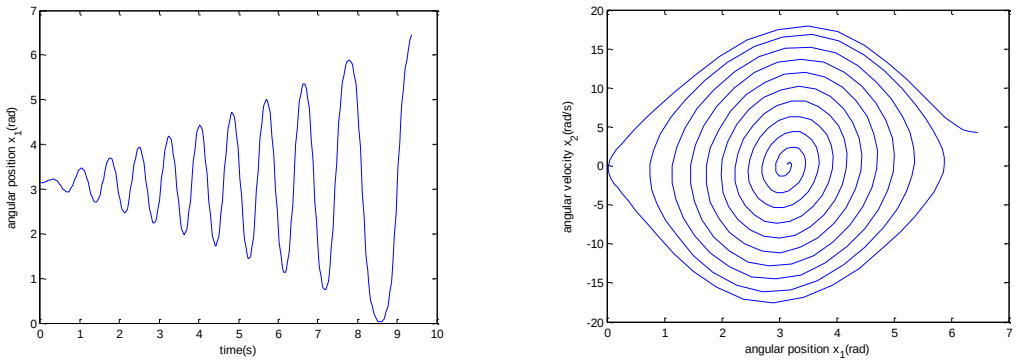

(a) (b)

Figure 17：Experiment results, excited by torque 0.02 [Nm] from $(\pi, 0)$. (a) Experiment result of pendulum angular position (b) Experiment result of pendulum response in phase plane

Remark: The difference between experiment and simulation is caused by disturbance from wire, accuracy of initial conditions, limited encoder resolution, time delay of the controller, unmodeled dynamics, etc.

6.4.2 Catching

The catching zones are shown in Figure 7 and Figure 8. The catching simulation result with various initial conditions are shown in Figure 17. The pendulum swings up from different initial conditions and reaches the trajectory s_0 described in Equation (12) in different locations. They are able to maintain within the boundaries and move to $(0,0)$ or $(2\pi, 0)$ along s_0.

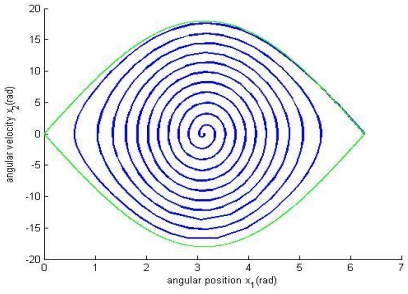

a) Initial condition $(\pi, 0)$

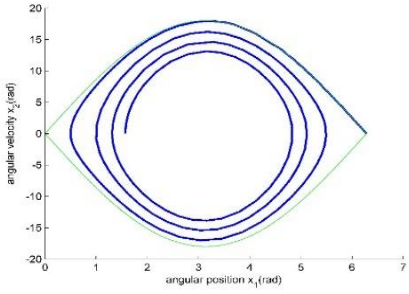

b) Initial Condition $\left(\frac{\pi}{2}, 0\right)$

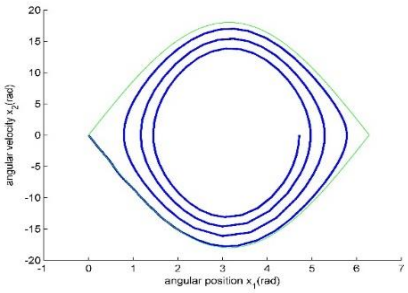

c) Initial Condition $\left(\frac{3\pi}{2}, 0\right)$

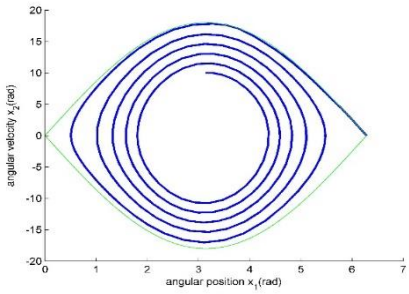

d) Initial Condition $(\pi, 10)$

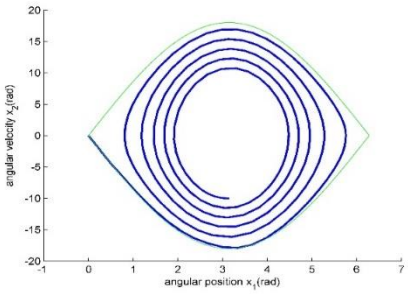

e) Initial Condition $(\pi, -10)$

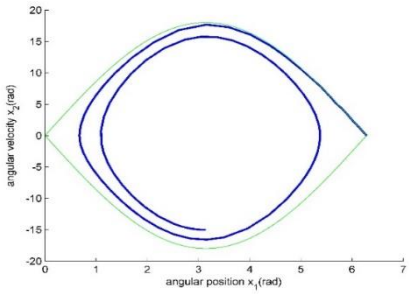

f) Initial Condition $(\pi, -15)$

Figure 18：Catching simulation result from different initial conditions. The green line describes the trajectory s_0 in Equation (12). The blue line shows the pendulum is caught into the trajectory s_0 from different swing-up initial conditions. All swing-ups are excited by $\tau_0 = 0.02$ [Nm].

6.4.3 Stabilization

Stabilization controller is activated to stabilize the pendulum around point (0, 0) or $(2\pi, 0)$. The simulation result is shown in the Figure 18

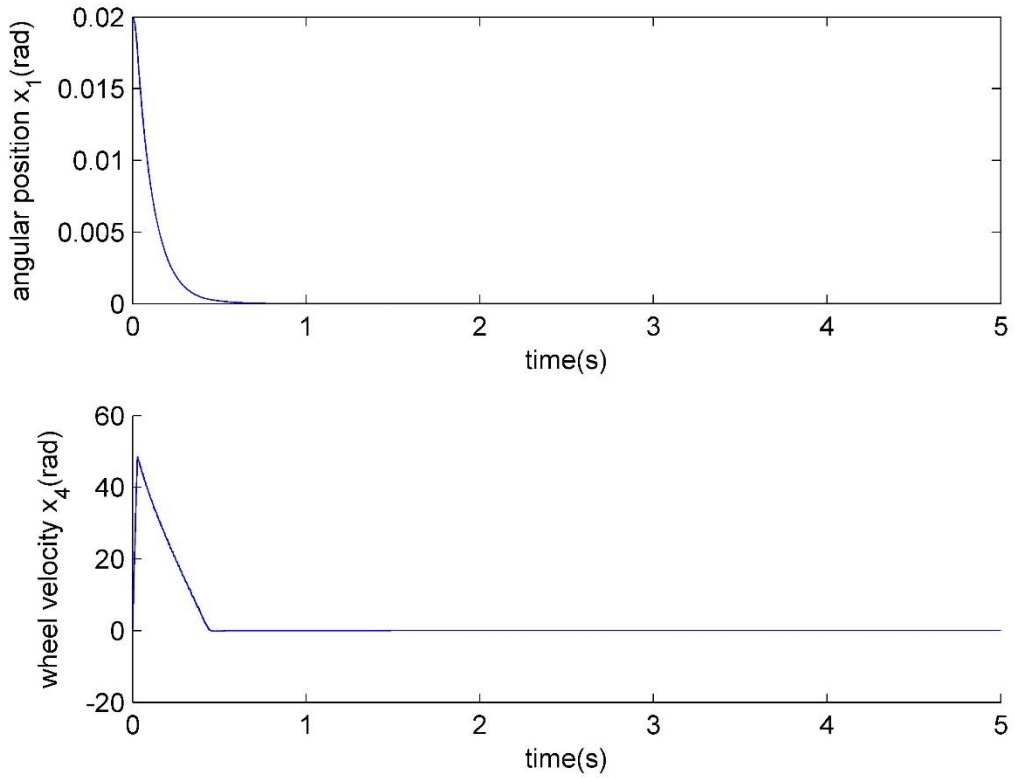

Figure 19：Stabilization simulation result: The pendulum stabilizes around (0, 0) from initial conditions (0.02, 0). From top to bottom: (1) The response of angular positon x_1 response. (2) The response of wheel velocity x_4. The simulation result shows that both angular position and wheel velocity can be kept at zero when no disturbances or noises applied.

We find that the system will lose the stabilization after a while due to high wheel velocity in the experiment. To maintain a constant torque ($\tau \neq 0$), the motor will need to accelerate and it will saturate ultimately. It is required to reduce the motor speed and try to keep it near zero. To deal with this trade off relationship between pendulum stabilization and wheel velocity, Block [1] added the wheel velocity error into his feedback control.

$$u = -k_{pp}\theta - k_{dp}\dot{\theta} + k_{dr}(\omega_{ref} - \omega)$$

By tuning 3 parameters (k_{pp}, k_{dp}, k_{dr}), he was able to find a good combination to solve this trade off problem and achieve both stabilization and zero wheel velocity.

In our experiment, a simple modification to the reference signal will make the system stabilization successful. Let $r(t) = 0.01\text{sgn}(x_4)$, the pendulum will have a tendency to oscillate around the upright position, effectively achieving a limit cycle. It makes the torque change direction all the time and helps to achieve boundness of wheel velocity. The experiment result of pendulum angle x_1 is shown in Figure 19. The experiment result of wheel velocity x_4 is shown in Figure 20. It is noticed that the response is noisy so that we applied a low pass filter. The filtered result is shown in Figure 21.

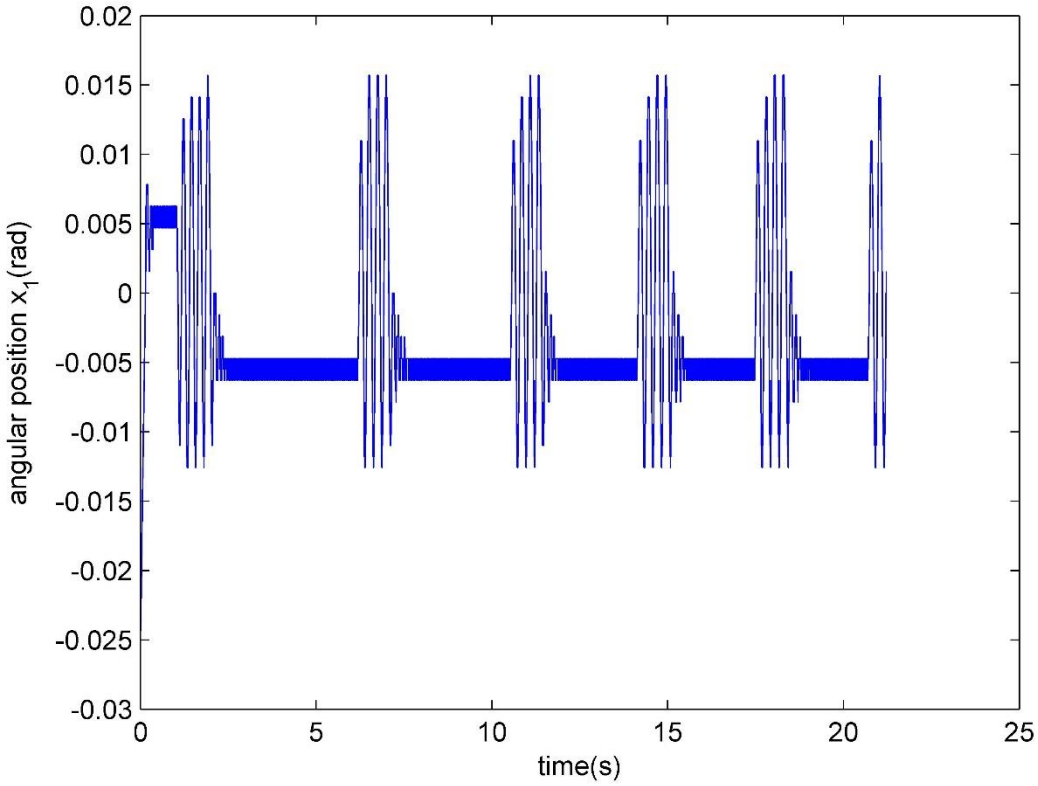

Figure 20：Stabilization experiment result of pendulum angular position x_1. It can be seen that the pendulum is able to achieve stabilization around upright position and limit cycle bang-bang (nonlinear) control. Chattering is due to encoder resolution limit.

6.4.4 Combined Strategy

By combining the 3 strategies, we can bring the pendulum from the bottom position to the upright positon. Simulations and experiment results from two initial condition have been compared. (1) $x_1 = \pi, x_2 = 0$ The simulation results are shown in Figure 22 and Figure 23. The experiment results are shown in Figure 24-26. (2) $x_1 =$

$2.586, x_2 = 0$ The simulation results are shown in Figure 27 and Figure 28. The experiment results are shown in Figure 29-31. In both initial conditions, the pendulum swings up by a switching control law described in Equation (8) with $\tau_0 = 0.15[\mathrm{Nm}]$. And then it is caught into the trajectory s_0 and move toward $(0,0)$. At last, it is able to be stabilized there.

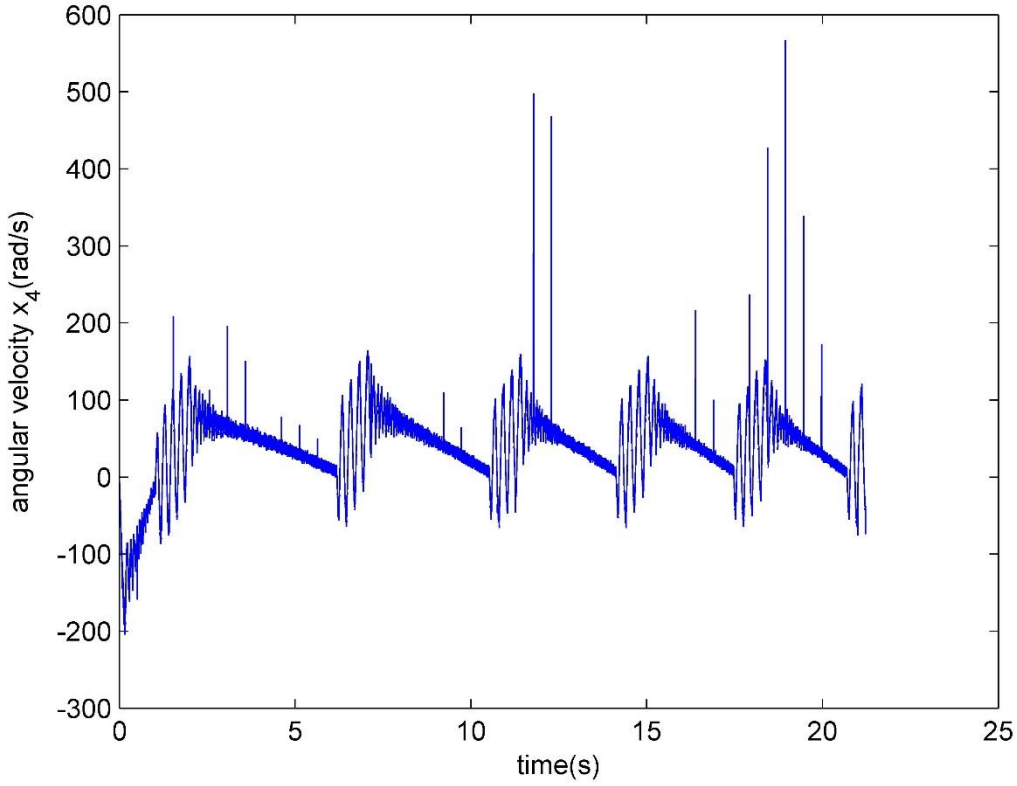

Figure 21：Stabilization experiment result of wheel velocity. It is shown that the wheel velocity it bounded but the signal is very noisy.

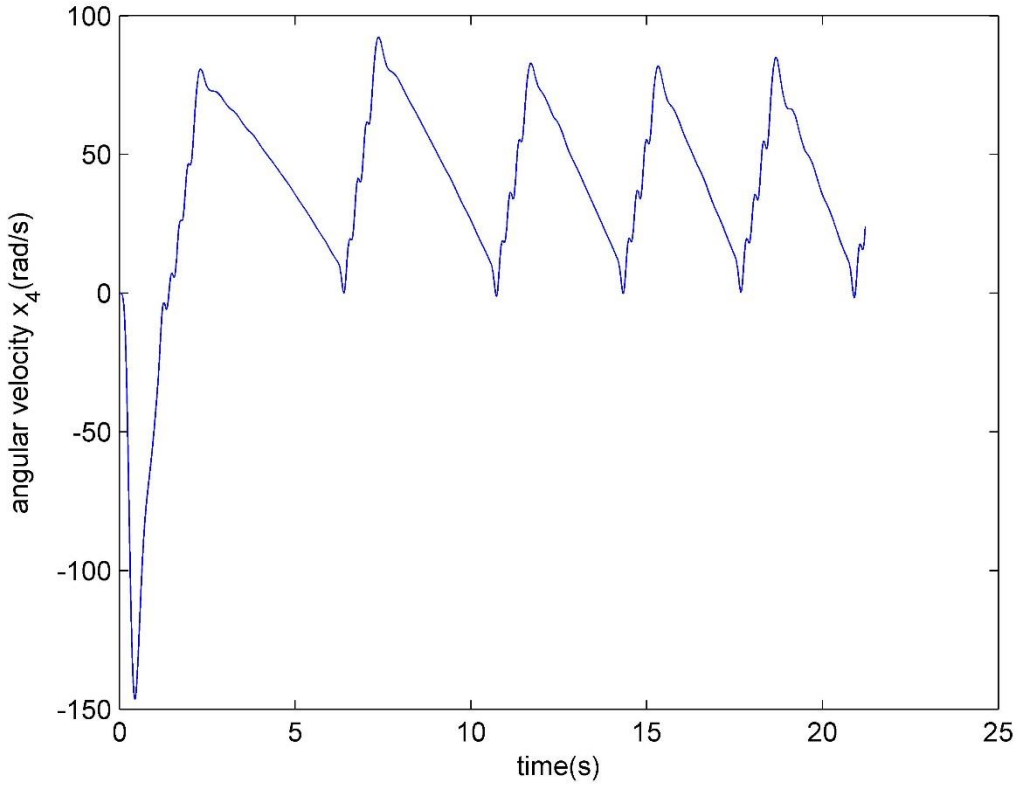

Figure 22：Stabilization experiment result of wheel velocity after applying a low pass filter. The filter is a 4th order low pass Butterworth filter with cutoff frequency 2 [Hz]. We can see that the wheel velocity x_4 is bounded.

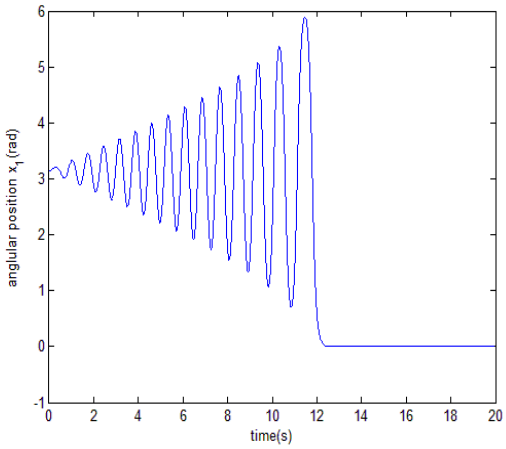

Figure 23：Combined strategy simulation result of pendulum angle x_1 from initial condition $x_1 = \pi, x_2 = 0$

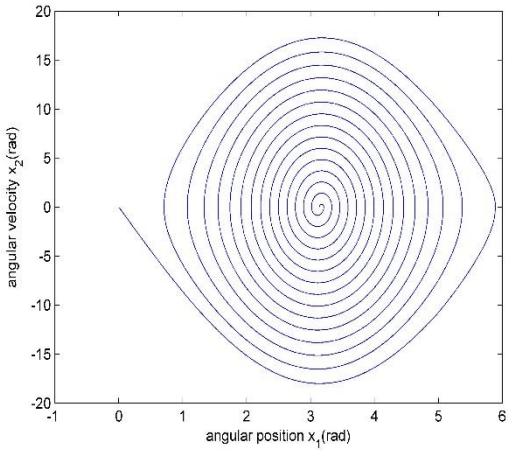

Figure 24：Combined strategy simulation result of pendulum angle x_1 and pendulum angular velocity x_2 in phase plane from initial condition $x_1 = \pi, x_2 = 0$

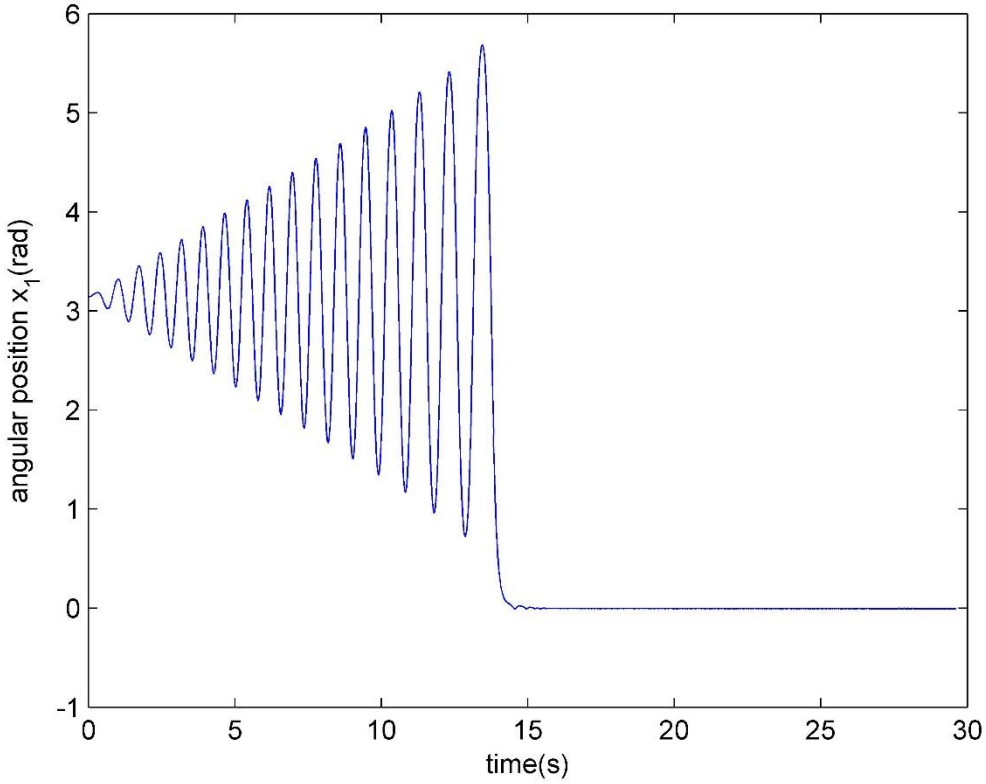

Figure 25：The experiment result of angular position x_1 in combined strategy from initial condition $x_1 = \pi, x_2 = 0$

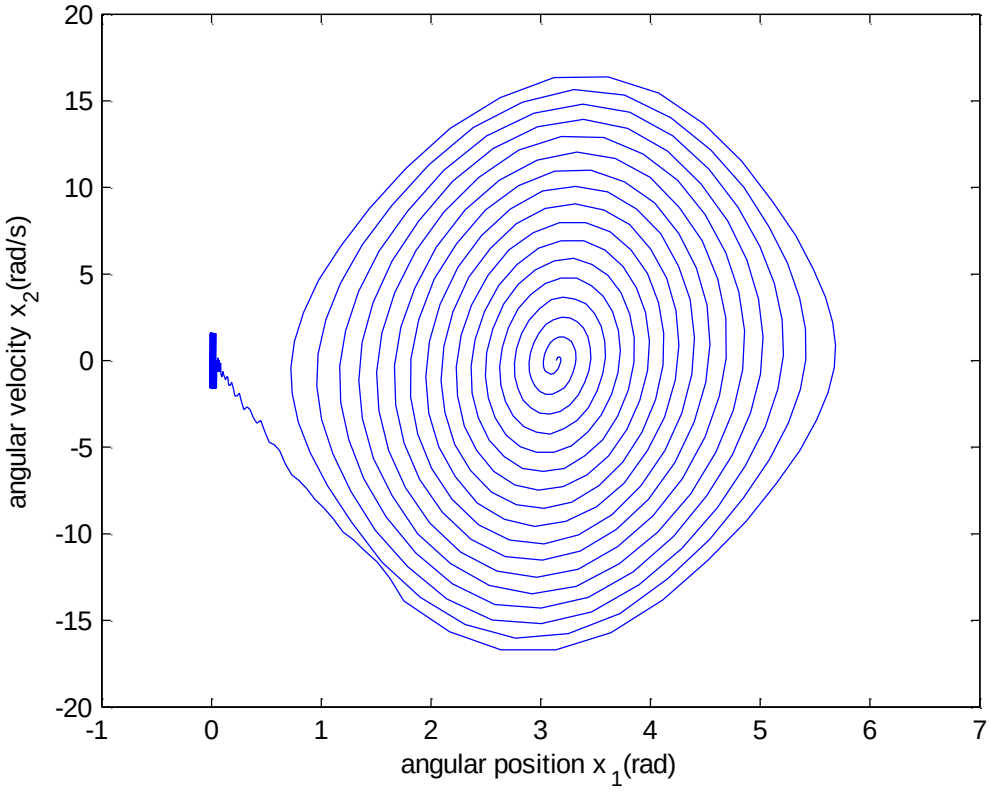

Figure 26：The experiment result of pendulum angle and angular velocity in phase plane initial condition $x_1 = \pi, x_2 = 0$

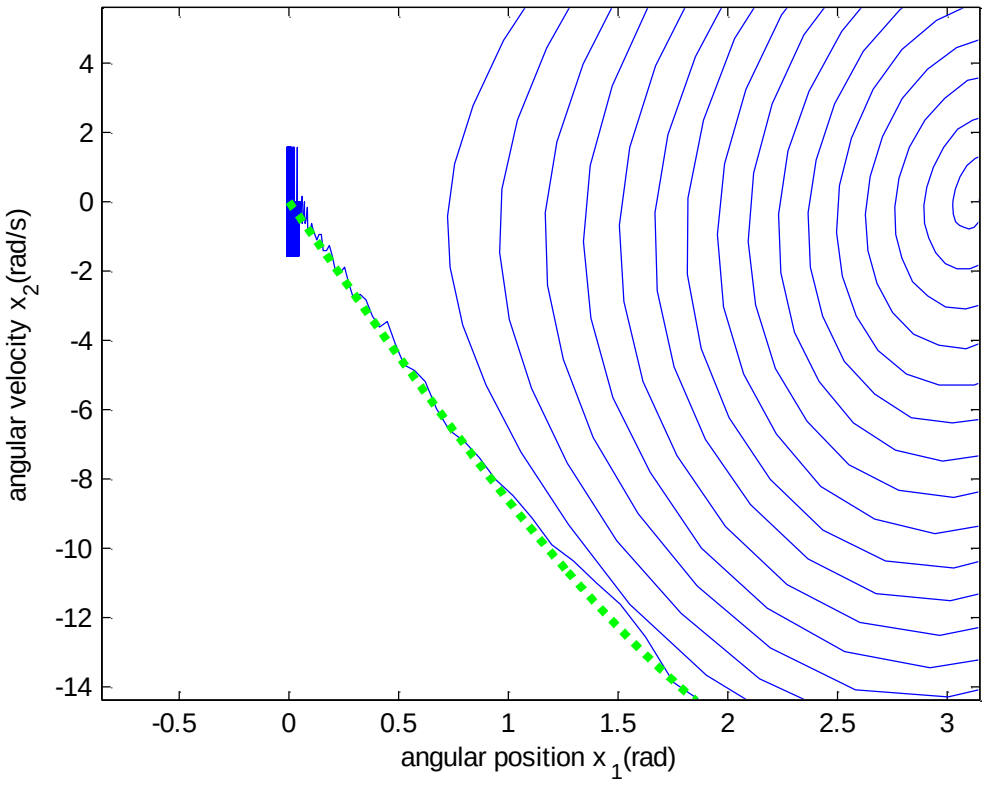

Figure 27：Zoomed-in view of stabilization around (0, 0) in the combined strategy initial condition $x_1 = \pi, x_2 = 0$. The green dotted line represents the trajectory s_0 in Equation (12)

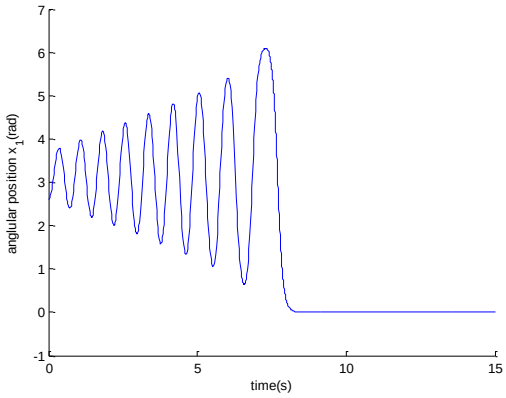

Figure 28：Combined strategy simulation result of pendulum angle x_1 from initial condition $x_1 = 2.586, x_2 = 0$

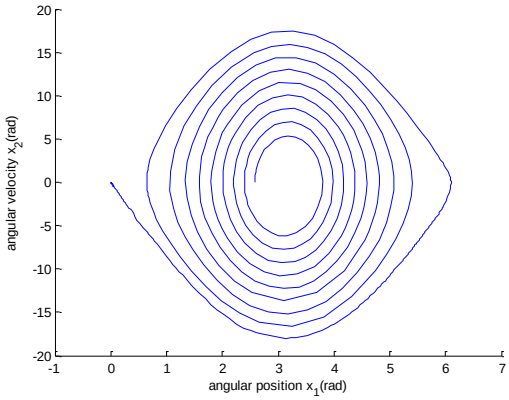

Figure 29：Combined strategy simulation result of pendulum angle x_1 and pendulum angular velocity x_2 in phase plane from initial condition $x_1 = 2.586, x_2 = 0$

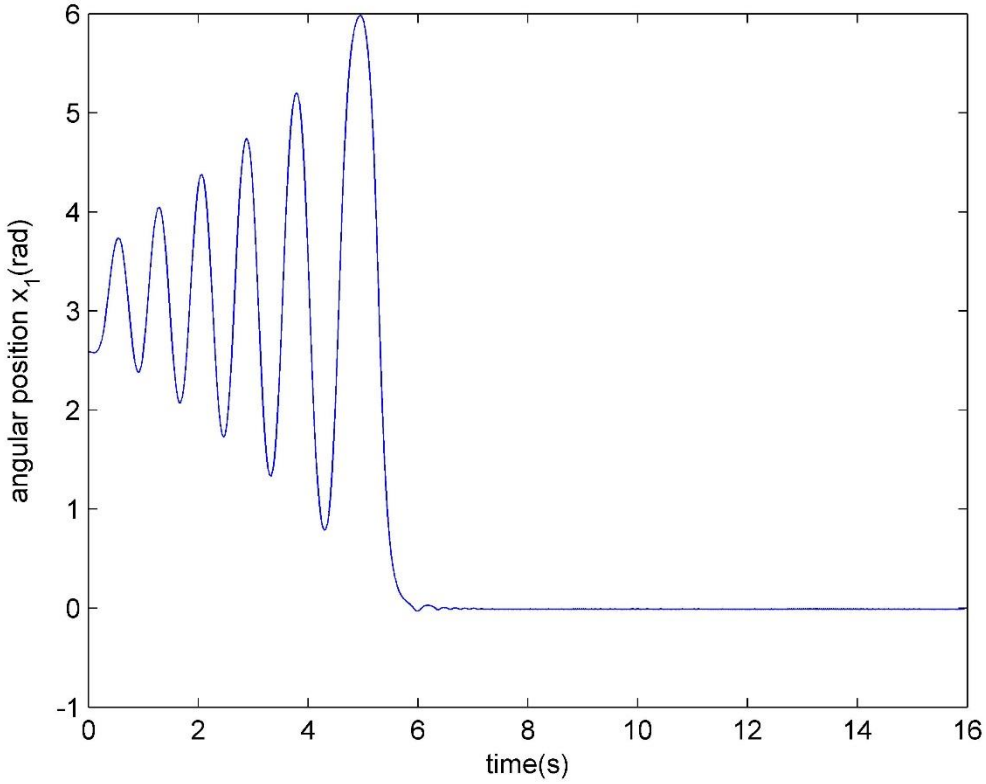

Figure 30：The experiment result of pendulum angle x_1 in combined strategy from initial condition $x_1 = 2.586, x_2 = 0$

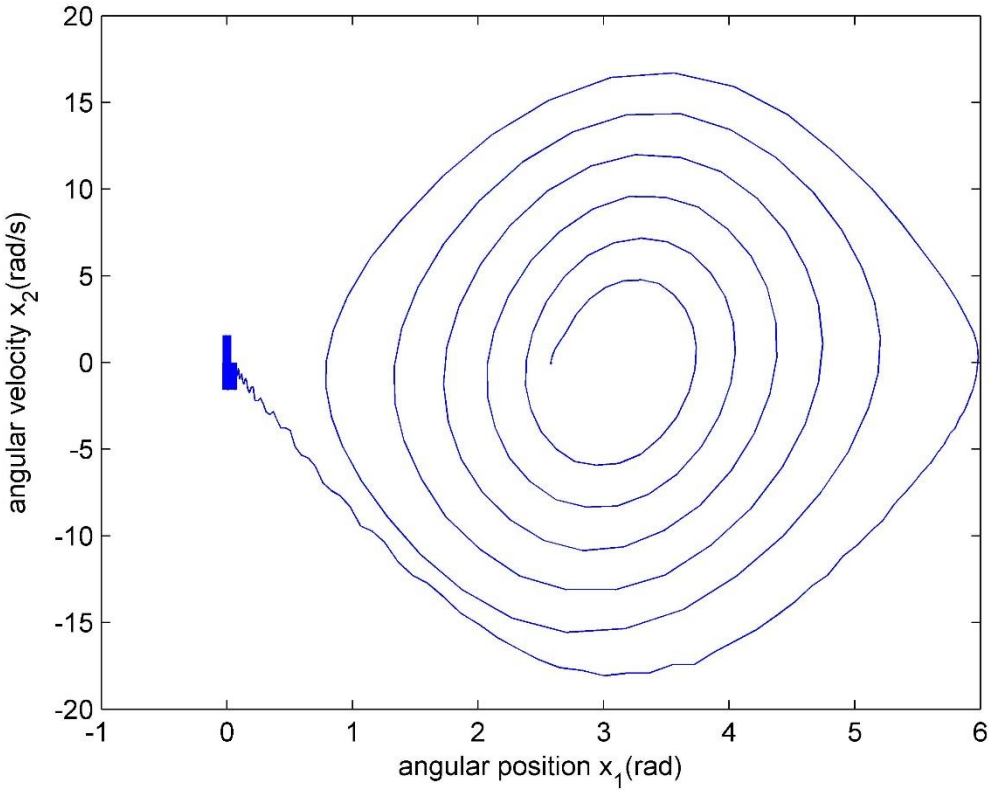

Figure 31：The experiment result of pendulum angle and angular velocity in phase plane initial condition $x_1 = 2.586, x_2 = 0$

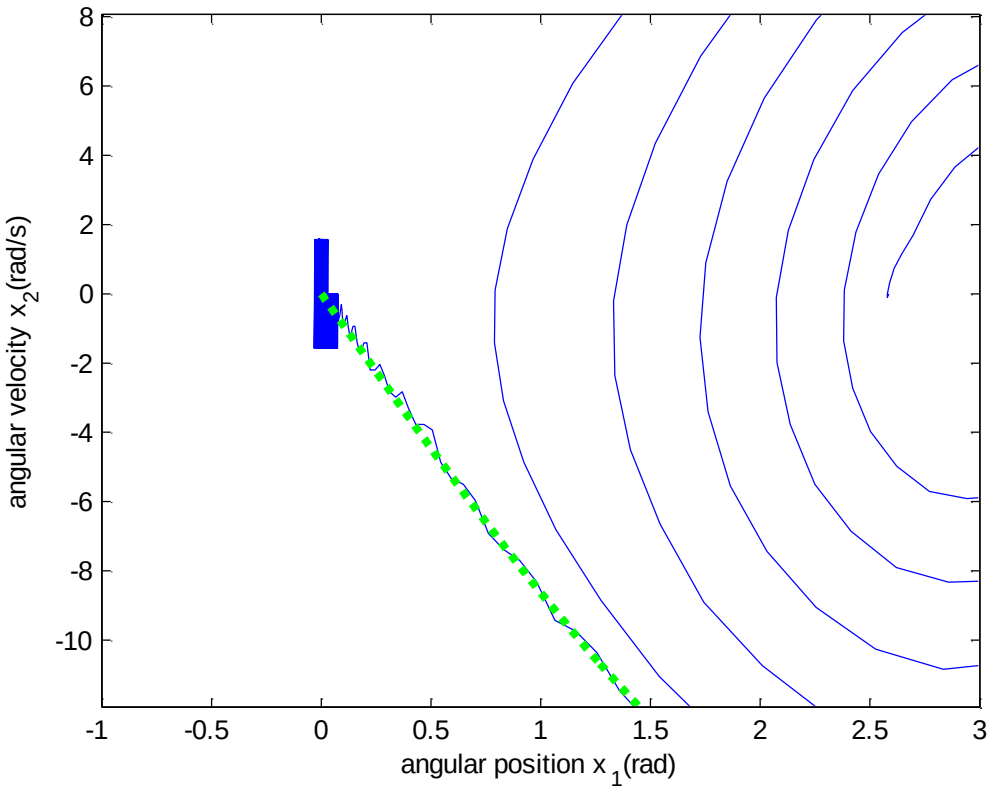

Figure 32：Zoomed-in view of stabilization around (0, 0) in the combined strategy initial condition $x_1 = 2.586, x_2 = 0$. The green dotted line represents the trajectory s_0 in Equation (12)

Chapter 7: Conclusion and Future Work

7.1 DISCUSSIONS

This section briefly compares our result with the previous methods. In the swing-up phase, our method can approach the upright position in approximately 4.5 seconds; similar to the result in [1]. However, the previous method requires lots of time to find a good combination of (k_e, k_v, k_u) to achieve satisfactory result [1]. Their method needs to be adjusted based on different experimental environments. There is no explicit solution of the RWP behavior under the energy/passivity-driven controllers. In contrast, our method does not require to tune many parameters and can be controlled along an explicit trajectory.

In the stabilization phase, the two methods indeed show similar results. However, if we install another motor with more torque we can broaden the stabilization angle range based on Equation (11) using our sliding mode controller but the previous method is not able to achieve this due to the limitations of linearization. Assume we choose a stronger motor Pittman 8843, the parameters of which are shown in Table 3. The comparison starting from an offset of 0.3 `[rad]` is shown in Figure 32-33, which illustrates that our method has more practical use for the future RWP-based applications.

Overall, the phase plane study in this thesis provides more predicable control process for the RWP and can be transferred to other robotics or nonlinear dynamic applications.

Table 3：Parameters of Pittman motor 8843

Parameter	Value	Unit
Terminal Resistance	2.74	Ohms
Inductance	2.57	mH
Peak Torque	0.3198	Nm
Torque Constant	0.037	Nm/A
Input Voltage	24	V

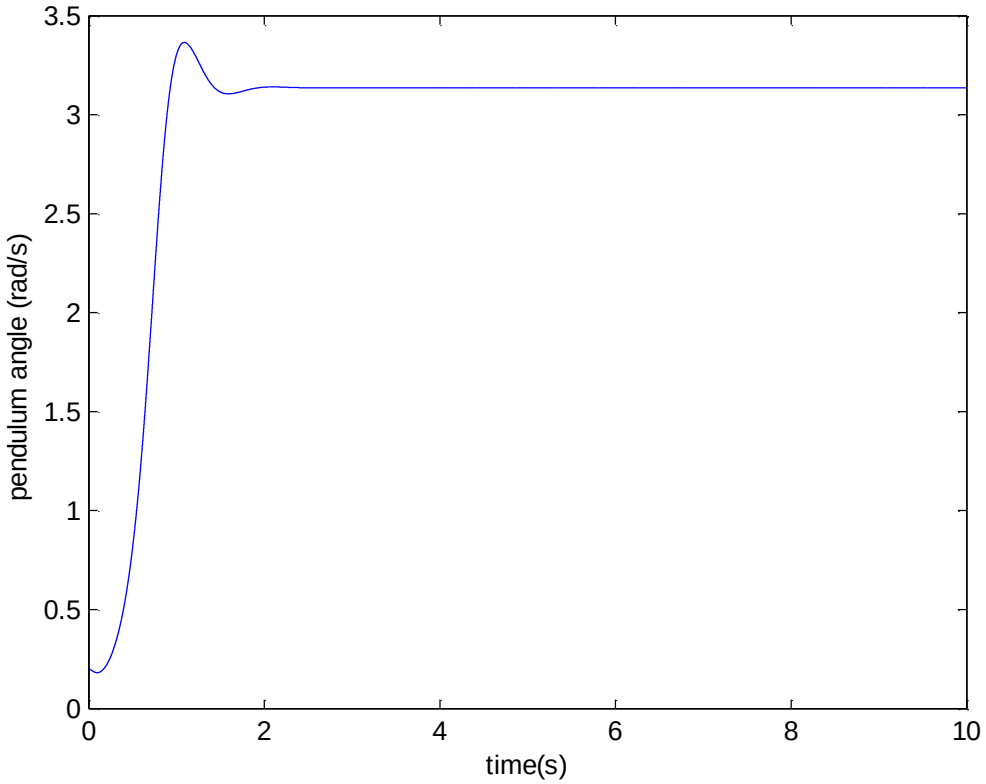

Figure 33：Simulation result of the traditional linearization method starting from 0.3 [rad] with a Pittman 8843 installed. It can be seen that the pendulum loses the stabilization shortly after start.

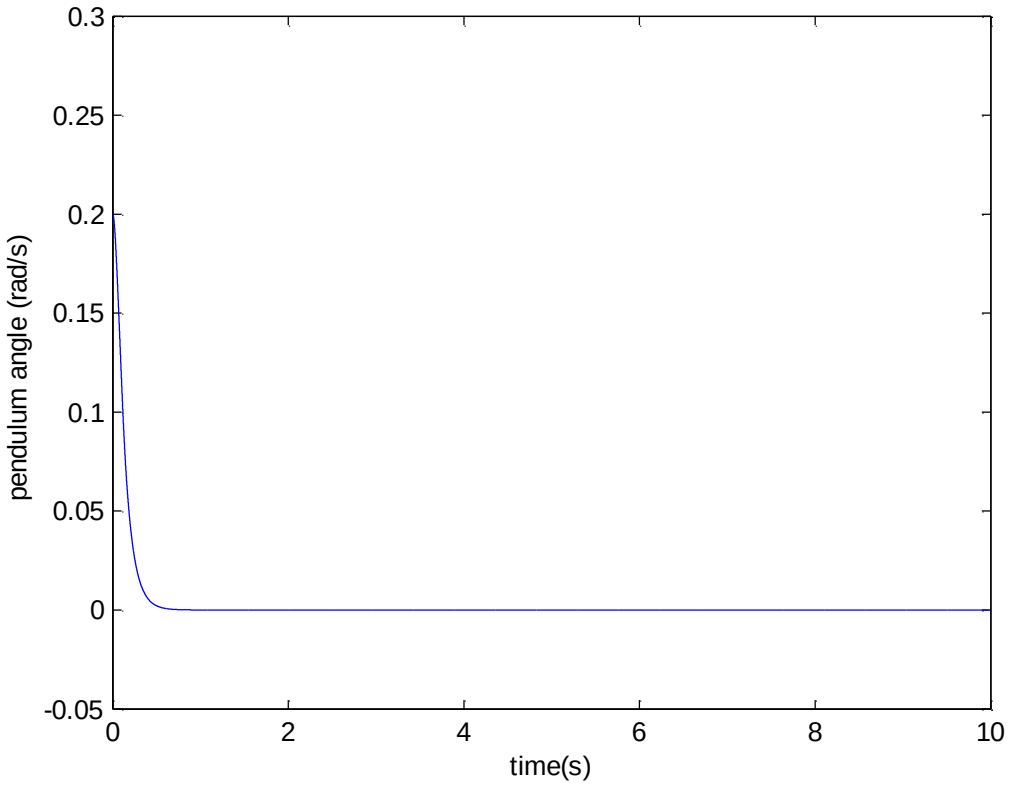

Figure 34：Simulation result of our sliding mode controller starting from 0.3 [rad] with a Pittman 8843 installed. It can be seen that the pendulum can maintain stabilization.

7.2 CONCLUSION

The Reaction Wheel Pendulum is a perfect tool to study the practice of nonlinear control theory. In this thesis, the dynamics of the RWP has been explained. Both the reduced 2nd order model and the 5th order model have been illustrated. We use the phase plane analysis to study the behavior of the RWP. The unactuated and actuated trajectories both have been explicitly explained. Three different strategies are combined

to control the pendulum in the upright positon from the bottom. The swing up strategy oscillates the pendulum by switching the direction of torque, which takes less time than other method such as energy method. A catching method is used to catch the pendulum when it reaches the trajectory that the unactuated pendulum swings from one upright position to another. A 2nd order sliding mode controller is used to maintain the pendulum moving along the trajectory. When it reaches the upright position, a 2nd order integral sliding mode controller is used to stabilize the pendulum or oscillate it in a limit cycle. We have conducted several experiments to find the parameters of the RWP, which is more accurate than using those calculated from the product specification due the installation error. This combined strategy has shown a good experiment result with less programming effort such as adaptive control or high gain observer.

7.3 FUTURE WORK

In this thesis, a 2nd order controller has been designed. We use an integral control in transition and sliding mode in stabilization to compensate the motor dynamics. There are different stabilization strategies that may be considered:

- 2nd order controller with PID control and high gain observers

The idea is to design a PID controller to compensate motor dynamics. Given that only angular position of motor and pendulum can be measured, it requires a high gain observer, which is introduced in [8]. One challenge in this method is to find an ideal PID controller parameters because the input torque is unpredictable.

- 4th order controller with high gain observers

Extend the sliding mode controller to 4th order based on equation (6) to directly compensate motor dynamics. But it requires much more programming effort and it is hard to find an ideal combination of observer gains.

Both methods require the design of high gain observers. The design of sliding mode controller with high gain observer was addressed in [9]. With a high gain observer, it is unavoidable to have a peak phenomenon which is undesired. Several approaches have been explored so far as in [10], [11] and [12].

Another interesting research is on the tracking problem. In this thesis, the stabilization controller is able to regulate the pendulum in the upright position but unable to tracking small amplitude trajectory such as a small amplitude sinusoidal motion. It is understood that the problem are caused by motor dynamics. The discontinuous term in sliding mode controller is able to compensate a regulation problem but it was unable to track a periodical reference signal. The future work may use the 2 different strategies discussed in the last chapter to solve a tracking problem. A periodical motion around upright position can be designed using method descried in [6] and a sliding mode control demonstration was introduced in [13].

Appendix A

Consider Equation (1)

$$\ddot{\theta} = a \sin\theta - b\tau$$

Rewrite

$$\frac{d^2\theta}{dt^2} = a \sin\theta - b\tau$$

Multiply $\frac{d\theta}{dt}$ on both side of the equation

$$\frac{d\theta}{dt}\frac{d^2\theta}{dt^2} = a\frac{d\theta}{dt}\sin\theta - b\tau\frac{d\theta}{dt}$$

Integrate on both side

$$\int \frac{d\theta}{dt}\frac{d^2\theta}{dt^2}dt = a\int \frac{d\theta}{dt}\sin\theta dt - b\tau\int \frac{d\theta}{dt}dt$$

$$\frac{1}{2}\dot{\theta}^2 = -a\cos\theta - b\tau\theta + c_1$$

Appendix B

Lie bracket of **f** and **g** is defined as

$$[\mathbf{f}, \mathbf{g}] = \nabla \mathbf{g}\, \mathbf{f} - \nabla \mathbf{f}\, \mathbf{g}$$

where $\nabla \mathbf{g} = \frac{\partial \mathbf{g}}{\partial \mathbf{x}}$, $\nabla \mathbf{f} = \frac{\partial \mathbf{f}}{\partial \mathbf{x}}$

$[f, g]$ can also be written as $\mathrm{ad}_{\mathbf{f}}\, \mathbf{g}$

And Lie bracket can be recursively defined as

$$\mathrm{ad}_{\mathbf{f}}^{i}\, \mathbf{g} = \left[\mathbf{f}, \mathrm{ad}_{\mathbf{f}}^{i-1}\, \mathbf{g}\right]$$

$$\mathbf{g} = \begin{bmatrix} 0 \\ 0 \\ 0 \\ 0 \\ \frac{k_e}{L} \end{bmatrix},\ \mathrm{ad}_{\mathbf{f}}^{1}\, \mathbf{g} = \begin{bmatrix} 0 \\ \frac{bk_e}{L} \\ 0 \\ -\frac{ck_e}{L} \\ \frac{Rk_e}{L^2} \end{bmatrix},\ \mathrm{ad}_{\mathbf{f}}^{2}\, \mathbf{g} = \begin{bmatrix} -\frac{bk_e}{L} \\ \frac{Rbk_e}{L^2} + \frac{bk_e\mu}{L} \\ \frac{ck_e}{L} \\ -\frac{Rck_e}{L^2} \\ \frac{R^2k_e}{L^3} - \frac{ck_e^3}{L^2} \end{bmatrix},$$

$$\mathrm{ad}_{\mathbf{f}}^{3}\, \mathbf{g} = \begin{bmatrix} -\frac{Rbk_e}{L^2} - \frac{bk_e\mu}{L} \\ \frac{abk_e \cos x_1}{L} + \mu\left(\frac{RbK_e}{L^2} + \frac{bk_e\mu}{L}\right) + b\left(\frac{R^2k_e}{L^3} - \frac{ck_e^3}{L^2}\right) \\ \frac{R_c k_e}{L^2} \\ -c\left(\frac{R^2k_e}{L^3} - \frac{ck_e^3}{L^2}\right) \\ \frac{R}{L}\left(\frac{R^2k_e}{L^3} - \frac{ck_e^3}{L^2}\right) - \frac{Rck_e^3}{L^3} \end{bmatrix},$$

$\mathrm{ad}_{\mathbf{f}}^{4}\,\mathbf{g} =$

$$\begin{bmatrix} -b\left(\frac{R^2k_e}{L^3}-\frac{ck_e^3}{L^2}\right)-\mu\left(\frac{RbK_e}{L^2}+\frac{bk_e\mu}{L}\right)-\frac{abk_e\cos x_1}{L} \\ a\cos x_1\left(\frac{Rbk_e}{L^2}+\frac{bk_e\mu}{2}\right)+b\left(\frac{R}{L}\left(\frac{R^2k_e}{L^3}-\frac{ck_e^3}{L^2}\right)-\frac{Rck_e^3}{L^3}\right)+\mu\left(b\left(\frac{R^2k_e}{L^3}-\frac{ck_e^3}{L^2}\right)+\mu\left(\frac{Rbk_e}{L^2}+\frac{bk_e\mu}{L}\right)+\frac{abk_e\cos x_1}{L}\right)-\frac{abk_ex_2\sin x_1}{L} \\ c\left(\frac{R^2k_e}{L^3}-\frac{ck_e^3}{L^2}\right) \\ -c\left(\frac{R}{L}\left(\frac{R^2k_e}{L^3}-\frac{ck_e^3}{L^2}\right)-\frac{Rck_e^3}{L^3}\right) \\ \frac{R}{L}\left(\frac{R}{L}\left(\frac{R^2k_e}{L^3}-\frac{ck_e^3}{L^2}\right)-\frac{Rck_e^3}{L^3}\right)-\frac{ck_e^2}{L}\left(\frac{R^2k_e}{L^3}-\frac{ck_e^3}{L^2}\right) \end{bmatrix}$$

$$\mathrm{C} = [\mathbf{g}, \mathrm{ad}_{\mathbf{f}}\,\mathbf{g}, \mathrm{ad}_{\mathbf{f}}^{2}\,\mathbf{g}, \mathrm{ad}_{\mathbf{f}}^{3}\,\mathbf{g}, \mathrm{ad}_{\mathbf{f}}^{4}\,\mathbf{g}]$$

C =

$$\begin{bmatrix} 0 & 0 & -711.0 & -1.4\times10^{6} & -5.8\times10^{4}\cos x_1 - 2.7\times10^{9} \\ 0 & 711.0 & 1.4\times10^{6} & 5.8\times10^{4}cos\,x_1 + 2.7\times10^{9} & 1.1\times10^{8}\cos x_1 - 5.8\times10^{4}x_2 sinx_1 + 5.1\times10^{12} \\ 0 & 0 & 1.7\times10^{5} & 3.3\times10^{8} & 6.4\times10^{11} \\ 0 & -1.7\times10^{5} & -3.3\times10^{8} & -6.4\times10^{11} & -1.2\times10^{15} \\ 4.3 & 8.3\times10^{3} & 1.6\times10^{7} & 3.1\times10^{10} & 6.0\times10^{13} \end{bmatrix}$$

with the parameter a and b we calculated in section 6.3 and those in Table 2. And

$c = \frac{1}{I_2} = \frac{1}{2.495\times10^{-5}} = 40080\,[\mathrm{rad/(Nm\cdot s^2)}]$, which is measured by Block [1] using

the same RWP product.

References

[1] D. Block, K. J. Astrom and M. W. Spong, The Reaction Wheel Pendulum, m. spong, Ed., Urbana: Morgan & Claypool, 2007.

[2] M. W. Spong, P. Corke and R. Lozano, "Nonlinear control of the Reaction Wheel Pendulum," *Automatica,* no. 37, pp. 1845-1851, 2001.

[3] R. Olfati-Saber, "Global Stabilization of a Flat Underactuated System: the Inertia Wheel Pendulum," in *Proceedings of 40th Conference on Decision and Control*, Orlando, 2001.

[4] K. Srinivas and L. Behera, "Swing-up control strategies for a reaction wheel pendulum," *International Journal of Systems Science,* pp. 1165-1177, 2008.

[5] B. Bapiraju, K. Srinivas, P. Prem kumar and L. Behera, "On Balanceing Control Strategies for a Reaction Wheel Pendulum," in *Proceedings of the IEEE INDICON*, IIT Kharagpur, India, 2004.

[6] L. Aguilar, I. Boiko, L. Fridman and L. Freidovich, "Inducing Oscillations in an Inertia Wheel Pendulum via Two-Relays Controller: Theory and Experiments," in *American Control Conference*, St. Louis, USA, 2009.

[7] J.-J. E. Slotine and W. Li, Applied Nonlinear Control, New Jersey: Prince-Hall Inc, 1991.

[8] H. Khalil, Nonlinear Systems, 3rd ed., NJ: Prentice Hall, 2002.

[9] S. Oh and H. K. Khalil, "Nonlinear Output-Feedback Tracking Using High-gain Observer and Variable Structure Control," *Automatica,* vol. 33, no. 10, pp. 1845-1856, 1997.

[10] A. A. Ball and H. K. Khalil, "High-Gain Observers in the Presence of Measurement Noise: A Nonlinear Gain Approach," in *Proc.IEEE Conf.Decision Contr.*, Cancun, 2008.

[11] J. H. Ahrens and H. K. Khalil, "High-gain observers in the presence of measurement noise: A switched-gain approach," *Automatica,* vol. 45, no. 4, pp. 936-943, 2009.

[12] A. A. Prasov and H. K. Khalil, "A Nonlinear High-Gain Observer for Systems With Measurement Noise in a Feedback Control Framework," *IEEE Transactions on Automatic Control,* vol. 58, no. 3, pp. 569-580, March 2013.

[13] V. Juarez, L. T. Aguilar and R. Iriarte, "Tracking Control for Inverted Orbital Stabilization of Inertia Wheel Pendulum-Trajectory Generation, Stability Analysis, and Experiments," in *Electrical Engineering Computing Science and Automatic Control (CCE), 2011 8th International Conference on*, Merida City, Oct 2011.

[14] R. Krishnan, Electric motor drives: modeling, analysis and control, New Jersey: Prentice Hall, 2001.

[15] L. Kovudhikulrungsri and T. Koseki, "Precise Speed Estimation From a Low-Resolution Encoder by Dual-Sampling-Rate Observer," *Mechatronics, IEEE/ASME Transactions on,* vol. 11, no. 6, pp. 661-670, December 2006.

[16] J. Travis and J. Kring, LABVIEW for Everyone: Graphical Programming Made Easy and Fun (National Instruments Virtual Instrumentation Series), Prentice Hall PTR, 2006.

[17] R. H. Bishop, LABVIEW 8 student edition, Pearson Prentice Hall, 2007.

[18] R. C. Dorf and R. H. Bishop, Modern Control Systems, 9th ed., Prentice Hall, 2000.

[19] I. Fantoni and R. Lozano, Non-linear control for underactuated mechanical systems, Springer, 2002.

[20] M. W. Spong, "Energy Based Control Of A Class Of Underactuated Mechanical Systems," in *IFAC World Congress*, 1996.

[21] S. K. Spurgeon, "Sliding mode observers: a survey," *International Journal of Systems Science,* vol. 39, no. 8, pp. 751-764, 2008.

[22] V. Muralidharan, A. D. Mahindrakar and V. Sankaranarayanan, "A Constructive Method for Designing Higher Order Sliding Surfaces for Single-input Nonlinear System," *World Congress,* vol. 18, no. 1, pp. 3944-3949, 2011.

[23] K. J. Åström and K. Furuta, "Swinging up a pendulum by energy control," *Automatica,* vol. 36, no. 2, pp. 287-295, 2000.

[24] M. W. Spong and M. Vidyasagar, Robot dynamics and control, New York: Wiley, 1989.

[25] V. Utkin, . J. Guldner and S. Ma, Sliding mode control in electro-mechanical systems, vol. 34, CRC Press, 1999.

[26] L. Sentis and B. Fernandez, "CoM State-Space Cascading Manifolds for Planning Dynamic Walking in Very Rough Terrain," in *Dynamic Walking*, July 2011.